Research

New Phytologist

The YABBY gene *SHATTERING1* controls activation rather than patterning of the abscission zone in *Setaria viridis*

Yunqing Yu[1], Hao Hu[2], Daniel F. Voytas[3], Andrew N. Doust[2] and Elizabeth A. Kellogg[1]

[1]Donald Danforth Plant Science Center, 975 North Warson Road, St Louis, MO 63132, USA; [2]Department of Plant Biology, Ecology, and Evolution, Oklahoma State University, Stillwater, OK 74078, USA; [3]College of Biological Sciences, University of Minnesota, St Paul, MN 55108, USA

Author for correspondence:
Elizabeth A. Kellogg
Email: ekellogg@danforthcenter.org

Received: *14 April 2023*
Accepted: *14 June 2023*

New Phytologist (2023) **240:** 846–862
doi: 10.1111/nph.19157

Key words: abscission zone, auxin, chloroplast, *Setaria viridis*, *SHATTERING1*, *YABBY*.

Summary

- Abscission is predetermined in specialized cell layers called the abscission zone (AZ) and activated by developmental or environmental signals. In the grass family, most identified AZ genes regulate AZ anatomy, which differs among lineages. A YABBY transcription factor, *SHATTERING1* (*SH1*), is a domestication gene regulating abscission in multiple cereals, including rice and *Setaria*. In rice, *SH1* inhibits lignification specifically in the AZ. However, the AZ of *Setaria* is nonlignified throughout, raising the question of how *SH1* functions in species without lignification.
- Crispr-Cas9 knockout mutants of *SH1* were generated in *Setaria viridis* and characterized with histology, cell wall and auxin immunofluorescence, transmission electron microscopy, hormonal treatment and RNA-Seq analysis.
- The *sh1* mutant lacks shattering, as expected. No differences in cell anatomy or cell wall components including lignin were observed between *sh1* and the wild-type (WT) until abscission occurs. Chloroplasts degenerated in the AZ of WT before abscission, but degeneration was suppressed by auxin treatment. Auxin distribution and expression of auxin-related genes differed between WT and *sh1*, with the signal of an antibody to auxin detected in the *sh1* chloroplast.
- *SH1* in *Setaria* is required for activation of abscission through auxin signaling, which is not reported in other grass species.

Introduction

Abscission, or shattering, is a highly programmed process in which plants detach unwanted organs. Abscission occurs in specialized cell layers at the organ junction called the abscission zone (AZ). The AZ is predetermined in early development and is often histologically distinctive, with the cells nonlignified and noticeably smaller than adjacent ones, forming an inherent weak point for breakage. Upon developmental (e.g. senescence) or environmental (biotic and abiotic stresses) cues, abscission initiates by activating cell wall hydrolytic enzymes and degrading the cell wall, mainly the middle lamella, leading to cell separation (Patterson, 2001; Kim, 2014). Programmed cell death is also observed during abscission in some species (Bar-Dror *et al.*, 2011; Yu *et al.*, 2023).

Early differentiation and late activation of the AZ are controlled by different sets of genes (Patterson, 2001; Kim, 2014). Differentiation genes are often required for the small cell size and nonlignification of the AZ cells, as in the floral AZ and fruit dehiscence zone (DZ) of *Arabidopsis*, and fruit AZ of rice (Ferrándiz *et al.*, 2000; Liljegren *et al.*, 2004; Konishi *et al.*, 2006; Zhou *et al.*, 2012; Dong & Wang, 2015). AZ/DZ with similar morphologies may be regulated by conserved genes, such as the fruit DZs in Brassicaceae (Lenser & Theißen, 2013), while AZ/DZ with different morphologies are controlled by different gene sets, such as the floral AZ and fruit DZ in *Arabidopsis* and the morphologically diverse fruit AZs of Poaceae (the grass family; Kim, 2014; Dong & Wang, 2015; Yu *et al.*, 2020a). In grasses, fruit AZs present a range of anatomical characteristics, with some being fully lignified and others completely nonlignified; some have notably smaller cells in the AZ than the surrounding cells, whereas in others the cell sizes are uniform (Pourkheirandish *et al.*, 2015; Yu & Kellogg, 2018; Yu *et al.*, 2020b). Consistent with this histological diversity, most genes identified in grasses as regulating AZ differentiation apparently do so only in particular species or clades; these include *SHATTERING4* (*SH4*), *qSH1* and *SHATTERING ABORTION1* (*SHAT1*) in rice (Konishi *et al.*, 2006; Li *et al.*, 2006; Zhou *et al.*, 2012), *Non-brittle rachis 1* (*Btr1*) and *Btr2* in barley (Pourkheirandish *et al.*, 2015), *Btr1* in durum wheat (Avni *et al.*, 2017) and *LESS SHATTERING1* (*LES1*) in *Setaria viridis* (Mamidi *et al.*, 2020).

Activation of the AZ is regulated by the balance of hormonal signaling. In *Arabidopsis*, increasing or decreasing endogenous indoleacetic acid (IAA) concentration in the floral AZ delays or accelerates petal abscission, respectively, suggesting a negative role of auxin in abscission. Petal break strength is decreased in the auxin importer mutants *aux1*, *lax3* and their higher order

mutants (Basu *et al.*, 2013). The auxin signaling repressor *auxin response factor2* (*arf2*) mutant has delayed senescence and floral organ abscission (Ellis *et al.*, 2005). In contrast, ectopic expression of a gain-of-function semidominant allele of *IAA17/AXR3* in the floral AZ disrupts auxin signaling and abolishes abscission, indicating that low auxin signaling might also be necessary for abscission (Basu *et al.*, 2013). In addition, floral organ abscission was delayed in ethylene- or jasmonic acid (JA)-insensitive mutants, suggesting that ethylene and JA accelerate abscission (Patterson & Bleecker, 2004; Kim *et al.*, 2013).

In grasses, most identified AZ genes control differentiation and morphology of the AZ (Li & Olsen, 2016; Yu & Kellogg, 2018), but little is known about the activation of abscission. The roles of hormones in fruit abscission of grasses are also barely known. IAA inhibits floret abscission in excised spikelets of *Avena fatua*, abscisic acid (ABA) promotes it, while gibberellic acid (GA) and ethylene treatments have no effect (Sargent *et al.*, 1984). IAA but not GA suppresses abscission in *Panicum maximum* (*Megathyrsus maximus*) under certain conditions, but the effects can be different or even opposite, depending on the genotypes and experimental conditions (excised panicles in growth chambers vs intact plants in the field; Weiser *et al.*, 1979). Furthermore, the upstream regulation of hormonal signaling and balance in the AZ is unclear in any studied system.

SHATTERING1 (*SH1*) is a domestication gene responsible for the loss of shattering in sorghum (*Sorghum bicolor*), foxtail millet (*Setaria italica*), fonio (*Digitaria exilis*) and rice (*Oryza sativa* and *O. glaberrima*; Lin *et al.*, 2012; Lv *et al.*, 2017; Odonkor *et al.*, 2018; Li *et al.*, 2020; Liu *et al.*, 2022). *SH1* belongs to the *YABBY2* (*YAB2*) clade of *YAB* transcription factors, which play important roles in plant development. In *Arabidopsis*, *YAB* genes have conserved roles in abaxial specification of lateral organs (Bowman, 2000). The relationship between YABs and auxin signaling has been demonstrated in eudicots. In *Arabidopsis* higher order *Atyab* mutants, expression of the auxin-responsive element reporter *DR5* is reduced, and distribution of the auxin exporter PIN1 is altered in the leaf and embryo, resulting in abnormal leaf and vein development (Sarojam *et al.*, 2010). Similarly, the *DR5* signal is weaker in the pistil of *Mlyab* knockdown mutants in *Mimulus lewisii* (Ding *et al.*, 2021). Tomato SlYAB2b binds directly to the promoter of auxin-amido synthetase *GH3.8* and suppresses its expression in shoots of 3-wk old plants. Exogenous application of IAA decreases the expression of *GH3.8*, which is delayed in the *Slyab2b* mutant. The expression of *SlYAB2b* is also induced by IAA treatment (Sun *et al.*, 2020).

In rice, SH1 is required for early AZ differentiation by inhibiting lignification in the AZ, similar to the phenotypes reported in other rice shattering mutants such as *sh4*, *sh5* and *shat1* (Zhou *et al.*, 2012; Yoon *et al.*, 2014; Lv *et al.*, 2017; Li *et al.*, 2020). The AZ of *Setaria viridis* is different from that of rice as its AZ is not lignified in either the AZ or the surrounding tissues, raising the question of how SH1 regulates abscission in species with different AZ morphologies (Hodge & Kellogg, 2016; Yu *et al.*, 2020b). As part of their diversity survey of *Svsh1* in various accessions of *Setaria viridis*, Liu *et al.* (2022) knocked out *Svsh1* in the ME034 background. Comparing gene expression of entire panicles to those of controls, Liu *et al.* (2022) found eight lignin-related genes to be differentially expressed, with one of these, *Cinnamyl Alcohol Dehydrogenase 2* (*CAD2*), reported as a direct target of SvSH1. However, the AZ of *S. viridis* and that of its domesticated relative *S. italica* are never lignified (Hodge & Kellogg, 2016; Liu *et al.*, 2022), so it is unclear how the differential lignin gene expression reported for whole panicles may apply to the AZ.

In this study, we characterize cellular and physiological aspects of the AZ in the wild-type (WT) A10 background (hereafter WT) and *Svsh1* mutants in *S. viridis*. We show that lignin is unlikely to contribute to the nonshattering phenotype in *Svsh1*. *SvSH1* has little obvious effect on early differentiation of the AZ. However, *SvSH1* is required to activate abscission at later developmental stages, a process that involves auxin pathways and chloroplast degradation.

Materials and Methods

Generation of *sh1* mutants using CRISPR-Cas9

Spacer sequences (5′-AGTAATAGCATGCTGAACAT-3′ and 5′-TTGTGGGCATTGCACTAGCC-3′) were each synthesized as partially overlapping oligos. Oligos were phosphorylated with T4 polynucleotide kinase (New England Biolabs, Ipswich, MA, USA) and annealed by boiling and gradual cooling. Annealed and phosphorylated oligos were separately cloned into Gateway (Invitrogen) compatible backbones with TaU6 promoter in front of each sgRNA. These TaU6-sgRNA-containing vectors and a *Triticum aestivum* codon-optimized version of SpCas9-containing vector pJG80 (Gil-Humanes *et al.*, 2017) were Gateway cloned into pANIC10A (Mann *et al.*, 2012) per the manufacturer's instructions. Plant transformation in *S. viridis* A10 followed Van Eck *et al.* (2017).

Plant growth conditions

Seeds of WT and *sh1* mutants of *Setaria viridis* (L.) Beauv. were sown in Jolly Gardener potting soil and kept moist at 4°C in the dark for 2–3 wk to break seed dormancy. Plants were grown in a growth chamber with 12 h : 12 h, light : dark, light intensity of 300 μmol m^{-2} s^{-1}, day and night temperatures of 31°C and 22°C and relative humidity of 50%.

Histology, *in situ* hybridization and light microscopy

Paraffin sections were prepared as described (Yu *et al.*, 2020a). Sections were deparaffinized using Histo-Clear, rehydrated in an ethanol series and stained with 0.05% (w/v) Toluidine blue O (TBO) in water for 1 min, or 0.01% (w/v) Acridine Orange (AO) in water for 10 min, followed by rinsing in water with gentle agitation three times for 1 min each, dehydrated in 95% and 100% ethanol, cleared in NeoClear twice for 5–10 min each and mounted with Permount mounting medium. *In situ* hybridization was performed as described (Yu *et al.*, 2020a). Images of TBO staining and *in situ* hybridization were taken with a Leica DM750 LED Biological microscope with ICC50 camera module and Leica Acquire v.2.0 software (Leica Microsystems, Wetzlar, Hesse, Germany). Images

of AO staining were taken using a TCS SP8-X confocal microscope (Leica Microsystems) with excitation wavelength of 488 nm and emission wavelength window of 498–600 nm. Fluorescence of the epidermal layers of the AZ and whole pedicel region was quantified using FIJI (v.2.9.0) software (Schindelin *et al.*, 2012) with five biological samples per genotype per stage. Images of live spikelets and AZs were taken using a Leica M125 C stereo microscope mounted with a Leica DMC2900 camera. Brightness was adjusted as necessary for images for final presentation, with adjustments applied to all parts of the image.

Chlorophyll fluorescence quantification

Abscission zone tissues were dissected under a stereo microscope, submerged in 4% (w/v) paraformaldehyde (PFA) and 0.1% (v/v) Tween 20 in 0.1 M PIPES buffer (pH 7.4), vacuum infiltrated for 10 min and incubated overnight at 4°C. Samples were rinsed in 0.1 M PIPES buffer three times for 10 min each, followed by sucrose gradient infiltration consisting of 25, 33, 50, 66, 75% (v/v) of 2.3 M sucrose in pairs of mPrep/s™ Capsules (22 550; Microscopy Innovations, Marshfield, WI, USA) for at least 1 h at each concentration at room temperature, and 100% 2.3 M sucrose overnight at 4°C (Knapp *et al.*, 2012). Samples were transferred to Shandon Cryomatrix™ Frozen Embedding Medium (Thermo Fisher Scientific, Waltham, MA, USA) in Tissue-Tek Cryomold (Sakura Finetek, Torrance, CA, USA) on dry ice and kept at −80°C. Samples were trimmed using a Leica CM1950 cryostat (Thermo Fisher Scientific) to expose a smooth surface of the inner tissues, and stained with DAPI and Calcofluor White for 10 min diluted 500× and 1000× in ultrapure water, respectively. Next, the samples were mounted on a coverslip and imaged on a TCS SP8-X confocal microscope (Leica Microsystems) with an HC PL APO CS2 63×/1.20 water objective lens. DAPI and Calcofluor White were detected with excitation wavelength of 405 nm and emission wavelength window of 415–630 nm, and chlorophyll autofluorescence was detected with excitation wavelength of 649 nm and emission wavelength window of 660–780 nm. Average intensity of the chlorophyll in the AZ was quantified as for AO staining, using six biological samples per genotype per stage, with the left and right sides of the AZ measured separately.

Immunofluorescence

Cell wall immunofluorescence followed the procedure described in Yu *et al.* (2023). To calculate average wall intensity for each probe, the probe signal in the AZ was divided by the area of cell wall autofluorescence using FIJI (v.2.9.0; Schindelin *et al.*, 2012). Four biological samples per genotype per stage were used, with the left and right halves of the AZ measured separately.

Indoleacetic acid immunofluorescence followed the description in Avsian-Kretchmer *et al.* (2002) with modifications. Specifically, 30- and 38-d AZs were dissected and prefixed in freshly prepared 3% (w/v) aqueous 1-ethyl-3-(3-dimethylaminopropyl)-carbodiimide hydrochloride (EDAC, 341006; Sigma-Aldrich, St. Louis, MO, USA) in ultrapure water at RT for 2 h, then transferred to 4% (w/v) PFA in 0.1 M PIPES buffer and 0.1% (v/v) Tween 20, vacuum infiltrated for 10 min and kept at 4°C overnight. Samples were washed in 0.1 M PIPES three times, dehydrated in an ethanol series, embedded in paraffin and sectioned as described previously for *in situ* hybridization. For immunofluorescence, samples were deparaffinized, rehydrated and kept in 1× PBS for 20 min, followed by incubation in 2% (w/v) BSA in 1× PBS buffer for 1 h at RT. Mouse monoclonal anti-IAA antibody (A0855; Sigma-Aldrich) was diluted 1 : 500 in 1% (w/v) BSA and 1× PBS, applied to the samples and incubated at 4°C overnight. Samples were then washed in 1% (w/v) BSA in 1× PBS three times for 10 min and incubated in Alexa Fluor® 488 goat anti-mouse antibody (1 : 100 dilution) (Thermo Fisher Scientific) for 1 h at RT. The samples were rinsed in 1× PBS, mounted with 90% glycerol and imaged as described previously for chlorophyll fluorescence. Alexa Fluor® 488, cell wall and chlorophyll autofluorescence were detected with excitation wavelength of 499, 405 and 649 nm and emission wavelength windows of 509–585, 415–485 and 661–779 nm, respectively. Average intensity of IAA in the AZ was quantified as above, with six to ten biological samples per genotype per stage. Colocalization between IAA (green) and chlorophyll (red) signals was analyzed using plugin BIOP JACop implemented in FIJI.

Hormone treatment and tensile strength measurement

The main panicles of 28–31-d-old plants were submerged in 10 mM 1-naphthaleneacetic acid (NAA), 500 µM GA, N-1-naphthylphthalamic acid (NPA), 2,3,5- triiodobenzoic acid (TIBA), 4-biphenylboronic acid (BBo), 4-phenoxyphenylboronic acid (PPBo) or ABA, or 50 mg l^{-1} ethephon in ultrapure water with 0.01% silwet-77 for 15 min daily for 4–6 d. Samples treated with NAA, NPA, TIBA, GA and ethephon were measured after 4–6 d of treatment, and samples treated with BBo, PPBo and ABA were measured daily for 4 d after treatment. Panicles were collected and hung upside down from a Mark-10 model M3-2 force gauge, and tensile strength of the most mature spikelet and pedicel junction was measured by pulling off spikelets using forceps. Experiments were repeated two or three times, with 1–3 plants and 15 spikelets per plant measured per replicate.

Reactive oxygen species (ROS) staining

Plants were treated with water control, NAA or TIBA for 15 min for five consecutive days as described previously. AZs and surrounding tissues were dissected 4–6 d after treatment and prepared as described for chlorophyll quantification. Samples were incubated in 0.1% (w/v) 3,3′-diaminobenzidine (DAB) in water (pH 3.8) at room temperature (RT) for 2 h in the light. Samples were transferred into 95% (v/v) ethanol for 1 h at RT to remove chlorophyll, then rinsed and kept in water. Images were taken immediately with a ZEISS Axio Zoom.V16 Fluorescence Stereo Zoom Microscope (Zeiss, Oberkochen, Germany).

Transmission electron microscopy (TEM)

Samples for TEM were prepared as described in Yu *et al.* (2023) with modifications. Briefly, AZs at 31 and 38 d were dissected

and fixed in 2% (w/v) PFA and 2% (w/v) glutaraldehyde with 0.1% (v/v) Tween 20 in 0.1 M cacodylate buffer at pH 7.4 overnight at 4°C and postfixed in 1% (w/v) osmium tetroxide in cacodylate buffer for 3 h, followed by 1% (w/v) aqueous uranyl acetate at 4°C overnight and then 50°C for 2 h. Samples were dehydrated in a graded acetone series and embedded in Quetol 651 epoxy resin at 60°C for 48 h. Samples were sectioned at 60 nm using a Leica Ultracut UCT ultramicrotome, mounted on formvar/carbon film on slotted gold grids (FCF2010-Au-SB; Electron Microscopy Sciences, Hatfield, PA, USA), stained with lead citrate for 8 min and imaged using a Talos L 120C G2 with a CETA 16 M 4 K × 4 K CMOS camera (Thermo Fisher Scientific), and tile mapped with 2 s exposure time using MAPS 3 software (v.3.16) at 8500× (pixel size 1.72 nm) and with VELOX (Release 3.1) at 17 500× or 22 000× magnifications. Three to four AZs per stage per genotype were imaged.

RNA-Seq library construction and sequencing

RNA-Seq libraries were prepared as described in Yu *et al.* (2020a) with modifications. The AZ, tissues immediately above (lower part of the spikelet excluding reproductive tissues, U) and below (pedicel, L) of 21- and 31-d-old plants, and the AZ of 38-d-old plants were collected and frozen in liquid nitrogen. Three panicles and *c.* 40 AZs were sampled per replicate, and four biological replicates were collected. After grinding, total RNA was isolated using a PicoPure RNA Isolation Kit (Applied Biosystems, Waltham, MA, USA) for each tissue following the manufacturer's instructions. After quantification with a Qubit™ RNA High Sensitivity kit, *c.* 250 ng total RNA was used for generating 3′ mRNA-Seq libraries using QuantSeq 3′ mRNA-Seq Library Prep Kit FWD for Illumina (Lexogen, Vienna, Austria). Libraries were single-end sequenced at 100 nt in one lane on an Illumina NovaSeq 6000 instrument at the Roy J. Carver Biotechnology Center at the University of Illinois at Urbana-Champaign.

RNA-Seq analysis

Raw reads were trimmed and quality-filtered using TRIMMOMATIC v.0.35 (Bolger *et al.*, 2014) and mapped to the *S. viridis* A10 v.2.1 genome (Mamidi *et al.*, 2020). Reads were counted per gene using STAR v.2.7.3 (Dobin *et al.*, 2013). Differential expression was calculated in DESEQ2 (v.1.38.2) in R (v.4.2.2; Love *et al.*, 2014), with raw counts as input. Genes with normalized counts > 10 for at least three samples were kept for further analysis. Significant differentially expressed genes (DEGs) were defined as 1.5-fold difference and adjusted *P*-values lower than 0.05. 1611 DEGs between genotypes were then clustered using Self-Organizing Map (SOM) in the R package KOHONEN (v.3.0.11; Wehrens & Buydens, 2007). The R package CLUSTERPROFILER (v.4.6.0) was used for gene ontology (GO) enrichment analysis (Wu *et al.*, 2021). Scripts with detailed parameters are available at https://github.com/Yunqing-Yu/sh1-AZ. Genes annotated as being auxin and cell wall related were identified based on annotation of the *Setaria viridis* genome (v.2.1) available on PHYTOZOME v.13 (https://phytozome-next.jgi.doe.gov/; Mamidi *et al.*, 2020) and cross-referenced with TAIR (https://www.arabidopsis.org/), PFAM (https://www.ebi.ac.uk/interpro/), GO annotation (http://geneontology.org/), KEGG (https://www.genome.jp/kegg/) and CAZy (http://www.cazy.org/) databases and literature (Boerjan *et al.*, 2003; Mohnen, 2008; Scheller & Ulvskov, 2010; Weng & Chapple, 2010; Atmodjo *et al.*, 2013; Zhong & Ye, 2015; Polko & Kieber, 2019; Vanholme *et al.*, 2019).

Prediction of promoter-binding motifs

Two-kilobyte upstream promoter sequences were extracted from the *Setaria viridis* genome (v.2.1; Mamidi *et al.*, 2020). The five previously reported YABBY-binding motifs from *Arabidopsis* and soybean (Shamimuzzaman & Vodkin, 2013; Franco-Zorrilla *et al.*, 2014; O'Malley *et al.*, 2016) were mapped on both strands of extracted promoter sequences using the FIMO program in the MEME Suite (http://meme-suite.org), with default parameters (Bailey *et al.*, 2015).

Results

Grain shattering is abolished in *Svsh1* mutants

Svsh1 was disrupted with CRISPR-Cas9 in the A10 background using two guide RNAs, both targeting the 2nd exon. Three independent indel alleles resulted in a frameshift and early stop codons; the mutations were biallelic and confirmed by Sanger sequencing. *sh1-1* and *sh1-3* share a stop codon in the conserved Zinc Finger domain, while the stop codon of *sh1-2* is two codons after the Zinc Finger domain (Fig. 1a,b). *In situ* hybridization showed that *SH1* is expressed in the AZ, the glumes and the base of the fertile floret in WT A10, consistent with previous observations in the ME034 background (Yu *et al.*, 2020a). However, *SH1* expression is lower in the mutant (Supporting information Fig. S1).

As plants matured, tensile strength of the spikelet attachment to the panicle gradually dropped to zero in the WT, while tensile strength remained high in all three mutant alleles and the spikelets remained attached (Fig. 1c,d). In all mutant alleles, heading and anthesis are 1–2 d later than in WT. Spikelet number per primary branch, panicle length and plant height vary slightly among the mutant alleles, with *sh1-1* and *sh1-2* more similar to WT and *sh1-3* larger than WT (Tukey's honestly significance test (HSD), $P < 0.01$; Fig. S2; Table S1a–f).

To confirm that the phenotype is caused by the *SH1* mutation, *sh1-1* and *sh1-2* were crossed reciprocally, and tensile strength and panicle length were evaluated in their F1 progenies. All F1 plants resembled their parents, regardless of the direction of the cross (Tukey's HSD test, $P < 0.01$; Fig. S3; Table S1g,h). Together, these results confirmed that *SH1* caused the loss of shattering in the mutant, and also had a small effect on flowering time.

Cell anatomy is comparable between wild-type and *sh1* before abscission activation

To test whether *SH1* controls shattering via changes in the cell wall, the anatomy of the spikelets and AZ was compared between

New Phytologist

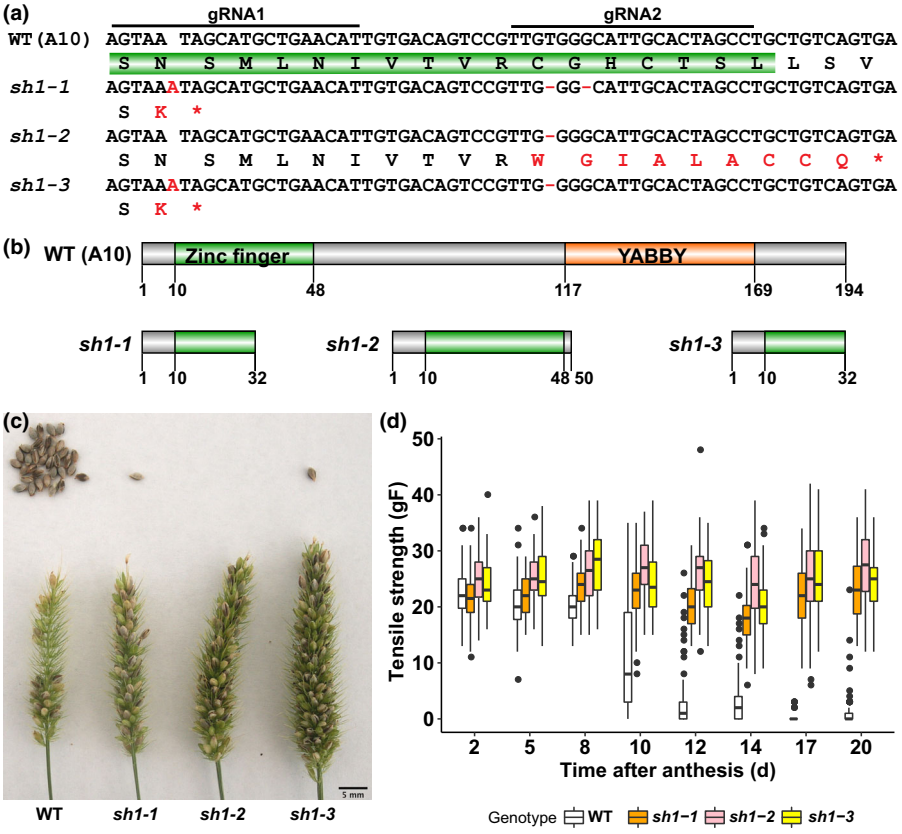

Fig. 1 Shattering is reduced in the *shattering1* (*sh1*) mutants of *Setaria viridis*. (a) DNA sequence alignments and the corresponding amino acid sequences of gRNA target sites in the second exon of *SvSH1*. DNA indels in the mutants are marked in red with letter 'A' denoting insertion and '-' denoting deletion. Mutated amino acids and stop codons are marked in red. Green shading in the amino acid sequence of wild-type (WT) marks part of the Zinc Finger domain. (b) Diagrams showing the length of SH1 protein and positions of Zinc Finger and YABBY domains in the WT and mutants. (c) Representative panicles with dropped seeds in WT and the three *sh1* mutant alleles. Bar, 5 mm. (d) Tensile strength measurements of spikelets in WT and *sh1* mutants. Values are 80 measurements per genotype per stage from four biological replicates. Elements in the boxplot: center line, median; box limits, upper and lower quartiles; whiskers, 1.5× interquartile range; black filled circles, outliers of individual tensile strength measurements.

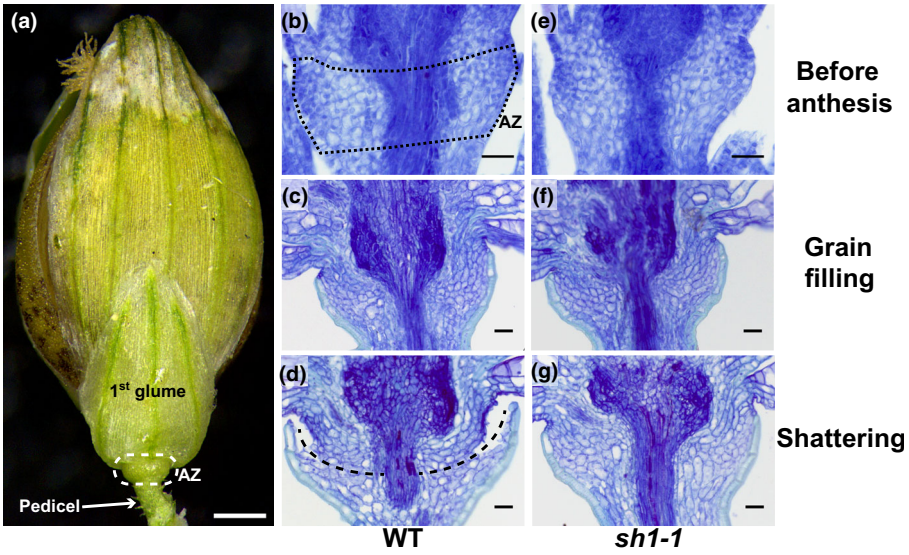

Fig. 2 Abscission zone (AZ) anatomy does not differ between wild-type (WT) and *shattering1-1* (*sh1-1*) of *Setaria viridis* until abscission is activated. (a) A representative image of a WT spikelet showing the position of the AZ (circle with white dotted lines) below the glumes. Bar, 200 μm. (b–g) Toluidine blue staining of the AZ of (b–d) WT and (e–g) *sh1-1* (b, e) before anthesis, at (c, f) grain filling and (d, g) shattering stages. Bars, 25 μm. (d) Curved dotted lines mark the location of cell separation.

WT and *sh1-1* using TBO staining. Spikelet anatomy was normal in the mutant, consistent with the putatively AZ-specific role of the protein (Fig. S4). The AZ itself also does not differ between WT and *sh1-1* until abscission occurs. In both genotypes, the AZ is nonlignified (stained blue), whereas the epidermal layer of the pedicel is lignified at grain filling and shattering stages (stained turquoise; Fig. 2). To quantify this result, the AZ was stained with the lignin stain AO (Li & Reeve, 2005). As in the TBO results, AO stained the epidermal layer as well as a few cells above or below the AZ, either in or near the vascular tissues (Fig. S5a–l). Signal intensity in the epidermis and in the upper pedicel including the AZ was not significantly different between the genotypes at either 30 d (grain filling) or 38 d (close to shattering; two-way ANOVA, $P > 0.05$; Fig. S5m; Table S1i).

We investigated whether other cell wall components of the AZ differed between WT and *sh1-1* using immunofluorescence.

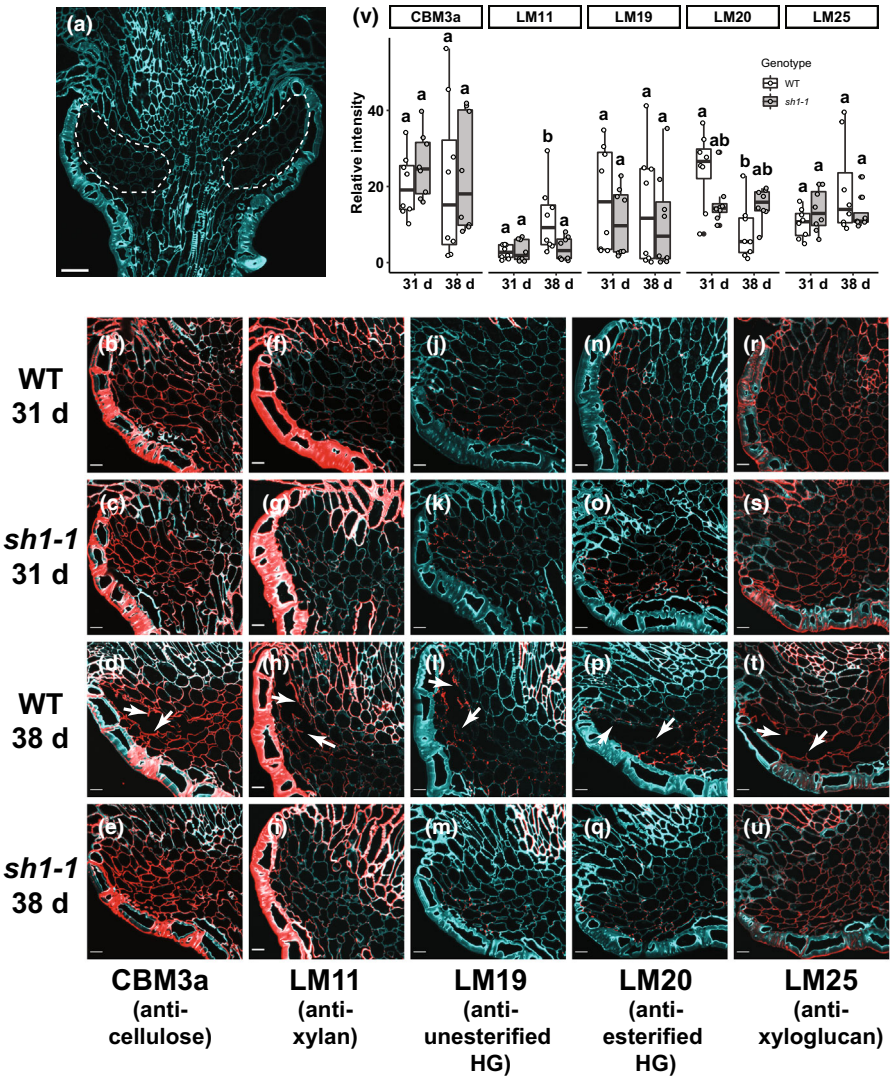

Fig. 3 Cell wall is modified during abscission in wild-type (WT) *Setaria viridis*. (a) Example of a confocal image of the WT abscission zone (AZ) using autofluorescence. Circles with white dotted lines mark the AZ regions for antibody signal quantification. Bar, 25 μm. (b–u) Representative images of immunofluorescence of the left half AZs probed with antibodies (b–e) CBM3a (anti-cellulose), (f–i) LM11 (anti-xylan), (j–m) LM19 (anti-unesterified homogalacturonan (HG)), (n–q) LM20 (anti-esterified HG) and (r–u) LM25 (anti-xyloglucan) in (b, d, f, h, j, l, n, p, r, t) WT and (c, e, g, i, k, m, o, q, s, u) *shattering1-1* (*sh1-1*) at (b, c, f, g, j, k, n, o, r, s) 31 d and (d, e, h, i, l, m, p, q, t, u) 38 d. Red, signal from antibody labeling; cyan, autofluorescence. Bars, 10 μm. (d, h, l, p, t) Arrows point to separated cells. (v) Quantification of fluorescence in the AZ. Circles are individual measurements as shown in (b–u). Elements in the boxplot: center line, median; box limits, upper and lower quartiles; whiskers, 1.5× interquartile range; black filled circles, outliers of individual measurements. $n = 8$ (2 × 4 biological samples per genotype per stage). Significant differences between genotypes and conditions (Tukey's HSD test, $P < 0.01$) are indicated with different letters.

Antibodies CBM3a, LM11, LM19, LM20 and LM25 were used to label cellulose, xylan, unesterified homogalacturonan (HG), esterified HG and xyloglucan, respectively. No differences were observed between WT and *sh1-1* at 31 d (grain filling), suggesting that SH1 does not affect cell wall composition early in development. WT plants at 38 d had more xylan and less esterified homogalacturonan than WT at 31 d. At 38 d, xylan signal in the WT is higher than that in *sh1-1* (Tukey's HSD test, $P < 0.01$; Fig. 3; Table S1j–n). These results suggest that the cell wall is modified during abscission activation in WT but not in *Svsh1* mutants.

Chloroplast degeneration precedes abscission

As no structural differences were observed in the AZ between WT and *sh1-1* before abscission, we hypothesized that *SH1* may be required to activate abscission rather than patterning the AZ itself. In WT, as the grain matured, the AZ and surrounding tissues gradually lost their chlorophyll. However, chlorophyll remained in the AZ of *sh1-1* even when the grain reached maturity (Fig. 4a–l). WT cells were intact at maturity, but had less chlorophyll signal than *sh1-1* (Student's *t*-test, $P = 4.87 \times 10^{-6}$; Fig. 4m–q), suggesting that the lack of chlorophyll was not due to cellular breakdown, but likely caused by chloroplast degeneration.

We examined subcellular changes during abscission with TEM. At 30 d in both genotypes, AZ cells were loosely packed with large intercellular spaces (Fig. 5a,e). The chloroplasts were intact, containing thylakoids, starch granules and plastoglobules (Fig. 5b–d,f–h). At 38 d, AZ cells of WT contained large vacuoles, with reduced volume of cytoplasm and organelles aggregated at the edges of cells, resembling morphologies in dying cells (Fig. 5i; van Doorn *et al.*, 2011). The chloroplasts were often irregularly shaped and lacked membrane integrity (Fig. 5i–l). Additionally, some cells appeared collapsed with concave cell walls, apparently initiating cell separation (Fig. 5i, arrow). In contrast, *sh1-1* had more organelles, including nuclei, chloroplasts and mitochondria, and cytoplasmic substance at 38 d. Chloroplasts were still intact and thylakoids were visible, although larger spaces between thylakoid membranes were

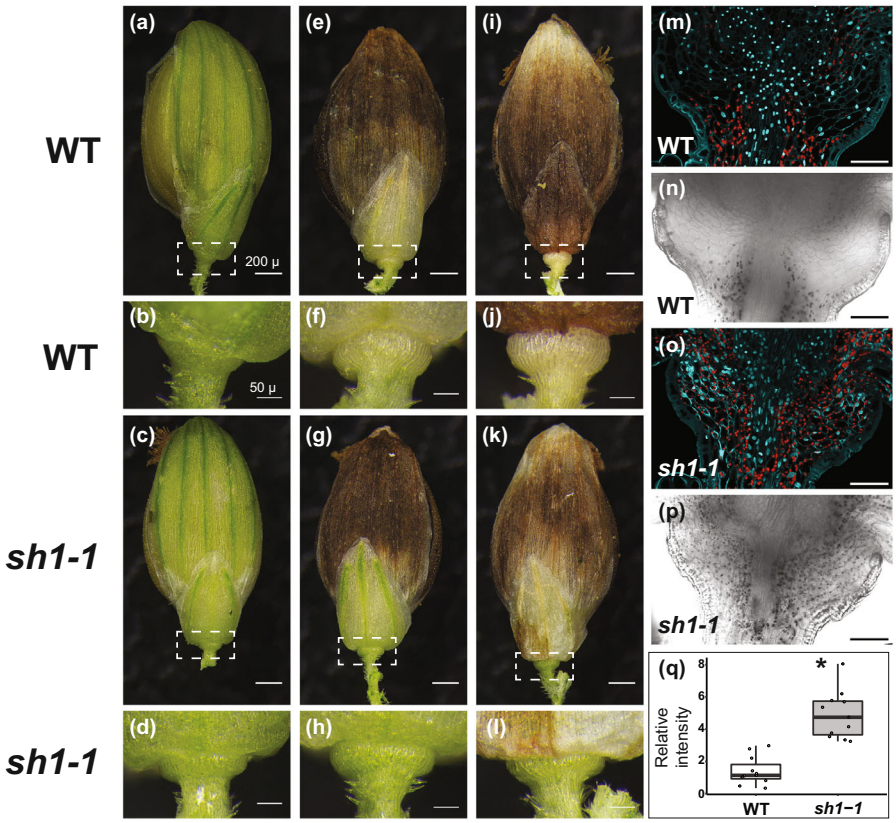

Fig. 4 Chlorophyll degenerates in the abscission zone (AZ) of wild-type (WT) *Setaria viridis* before abscission. (a–l) Representative images of (a, e, i, c, g, k) whole spikelets and (b, f, j, d, h, l) AZ of (a, b, e, f, i, j) WT and (c, d, g, h, k, l) *shattering1-1* (*sh1-1*). (a, e, i, c, g, k) Rectangular boxes with white dotted lines mark the zoomed AZ region. Bars, 200 μm. (b, f, j, d, h, l) Bars, 50 μm. (m–p) Representatives of (m, o) fluorescence and (n, p) transmitted light images of longitudinal views of AZ in (m, n) WT and (o, p) *sh1-1*. Bars, 50 μm. (m, o) Red color, chlorophyll autofluorescence; cyan color, DAPI and Calcofluor White signal. (q) Quantification of chlorophyll autofluorescence. Circles are individual measurements of half of the AZs. Elements in the boxplot: center line, median; box limits, upper and lower quartiles; whiskers, 1.5× interquartile range. $n = 10$ from six biological AZ samples per genotype. Star denotes a significant difference between the genotypes (Tukey's HSD test, $P < 0.01$).

observed than at 30 d (Fig. 5m–p). These results confirmed that *SvSH1* affects the activation of abscission, which involves chloroplast degeneration and likely cell death.

Auxin dynamics inhibit the production of ROS and abscission

As hormones may accelerate or delay abscission in other systems (Sexton & Roberts, 1982), we examined the effects of auxin, ethylene, GA and ABA on shattering in WT and *sh1-1*. In WT, both the synthetic auxin NAA and the auxin transport inhibitor TIBA increased the tensile strength holding spikelets on the panicle, although tensile strengths remained lower than in *sh1-1*. The effects of another auxin transport inhibitor, NPA, on WT varied and were not significantly different from the control. Conversely, no treatment affected the tensile strength of *sh1-1* (Tukey's HSD test, $P < 0.01$; Fig. 6a; Table S1o). We also tested the effects of auxin biosynthetic inhibitors, BBo and PPBo, which target the IAA biosynthetic enzyme YUCCA in *Arabidopsis* (Kakei *et al.*, 2015). Neither inhibitor affected shattering in either WT or *sh1-1* (Tukey's HSD test, $P < 0.01$; Fig. S6a; Table S1p). Similarly, GA had no effect on tensile strength in either genotype (Tukey's HSD test, $P < 0.01$; Fig. S6b; Table S1). Although ethylene and ABA are known shattering accelerators in some species (Sexton & Roberts, 1982; Sargent *et al.*, 1984), in our hands, both ethephon and ABA inhibited shattering in WT and had no effect on *sh1-1*. We also observed that both treatments affected grain development as the treated spikelets were often sterile, which may in turn affect shattering (Tukey's HSD test, $P < 0.01$; Fig. S6b,c; Table S1q,r).

NAA and TIBA treatments suppressed chloroplast degeneration in the AZ. Treated WT plants had more chlorophyll in the AZ, although it remained lower than that of *sh1-1* (Tukey's HSD test, $P < 0.01$; Fig. 6b–n; Table S1s). This result was consistent with the trend of spikelet tensile strength, suggesting that auxin might suppress chloroplast degeneration before initiation of abscission (Fig. 6a–n).

As ROS are released during chloroplast degradation (Woodson, 2022), we tested whether ROS accumulated in the AZ of WT. The H_2O_2 indicator DAB found no H_2O_2 accumulation in the AZ of either genotype. Instead, the tissue above the AZ was heavily stained in WT compared with *sh1-1* (Figs 6o, S7). Both NAA and TIBA treatments reduced H_2O_2 accumulation in WT, while no obvious difference was observed in *sh1-1* in any of the tested conditions (Fig. 6o–q). Together, these results place auxin signaling upstream of ROS production and chloroplast degradation, which may serve as signals to activate abscission.

IAA was localized in the chloroplast in *sh1-1* assayed by immunofluorescence

As auxin and the auxin transport inhibitor TIBA both suppress abscission in WT, we hypothesized that auxin distribution in the AZ may be important for its function. Accordingly,

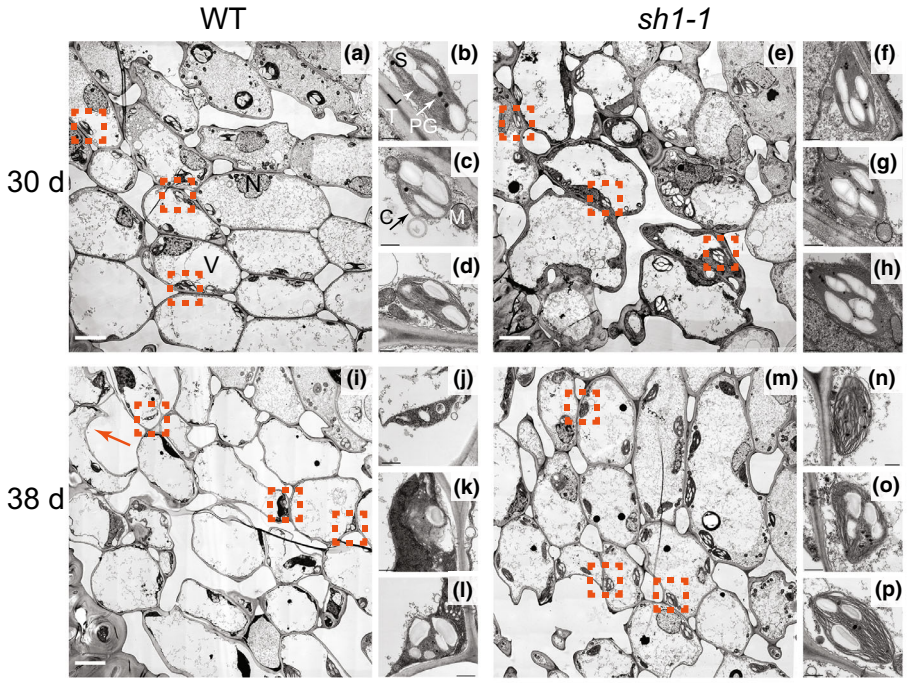

Fig. 5 Transmission electron microscopy reveals chloroplast degradation and cell death in the abscission zone (AZ) of wild-type (WT) *Setaria viridis* during abscission initiation. (a, e, i, m) Representative images of cells in the AZ of (a, i) WT and (e, m) *shattering1-1* (*sh1-1*) at (a, e) 30 d or (I, m) 38 d. Bars, 5 µm. N, nucleus; V, vacuole. (i) Arrow points to the concave cells that have separated from adjacent cells. (b–d, f–h, j–l, n–p) Enlarged images of chloroplasts marked in the orange boxes in (a, e, i, m). (b–d) WT at 30 d. (f–h) *sh1-1* at 30 d. (j–l) WT at 38 d. (n–p) *sh1-1* at 38 d. Bars, 500 nm. C, chloroplast; M, mitochondrion; PG, plastoglobules; S, starch; T, thylakoid.

immunofluorescence was used to visualize and quantify IAA (and possibly some conjugated derivatives) in the AZ (Leverone *et al.*, 1991; Avsian-Kretchmer *et al.*, 2002). While the auxin signal was reduced at 38 d compared to 30 d in both genotypes, the genotypes did not differ significantly at either time point (Tukey's HSD test, $P < 0.001$; Fig. 7a–m; Table S1t). However, auxin localization differed at the 38-d stage. The auxin signal (green) was mainly cytoplasmic in both genotypes at 30 d and in WT at 38 d (Figs 7a–c, S8). In contrast, in *sh1-1* at 38 d, the auxin signal overlapped with chlorophyll autofluorescence (magenta; Fig. 7n–p). Colocalization was quantified with Pearson's correlation coefficient (PCC) and Manders overlap coefficient (MOC; Dunn *et al.*, 2011). With both methods, at 38 d, the colocalized auxin (green) signal in *sh1-1* was significantly higher than in WT (Tukey's HSD test, $P < 0.001$; Fig. 7q; Table S1u–w), while colocalization between WT samples at 30 or 38 d or *sh1-1* at 30 d was not significantly different (Tukey's HSD test, $P > 0.01$; Fig. 7q; Table S1u–w). In other words, a higher proportion of auxin (green) signal overlapped with the chloroplast (magenta in Fig. 7o,p) signal at 38 d in *sh1-1*. Conversely, as the chloroplast signal was reduced in WT at 38 d, the ratio of overlapped signal to the chloroplast signal was the same between genotypes at both stages (Fig. 7q). Together, these results suggest that the subcellular distribution of auxin, rather than the total amount, differs between WT and *sh1-1* at 38 d close to abscission.

SH1 regulates gene expression in the AZ in late development

SH1 regulated genes were identified by RNA-Seq analysis of the AZ and the tissues immediately above (U, upper) and below (L, lower) it at 21 and 31 d (preheading and seed filling, respectively), and the AZ at 38 d (close to abscission; Fig. S9). At each stage, more genes were differentially expressed in the AZ than in U or L (Fig. 8a). In addition, more DEGs were identified in the AZ at 38 d (697 up and 622 downregulated genes) than at 21 or 31 d, consistent with the phenotype being mainly visible at the latest developmental stage (Fig. 8a; Table S2).

The 1611 DEGs were placed in nine clusters by Self-Organizing Map (SOM). SOM1-3 were similar between the two genotypes, SOM4, 5, 7 and 8 downregulated in *sh1-1*, and SOM6 and 9 upregulated in *sh1-1* (Fig. 8b). Consistent with the *in situ* hybridization results (Fig. S1) and the RNA-Seq data of Liu *et al.* (2022), *SH1* was in SOM5, in which gene expression was lower in the mutant in all tissue types and stages. The downregulation of *SH1* in the mutant was more pronounced as the plants matured, implying that the functional SH1 protein might be necessary to maintain its transcript level (Table S2). *LES1* was in SOM7, in which genes were upregulated at later stages in WT, but not as strongly in *sh1-1*, suggesting that *SH1* positively regulates *LES1* (Fig. 8b; Table S3).

Different sets of stress-related genes were upregulated in WT and *sh1-1* (Fig. 8c; Table S4). The top 10 enriched GO terms in SOM4, 7 and 8 included GO:0042542 (response to hydrogen peroxide), GO:0034976 (response to endoplasmic reticulum stress) and GO:0009408 (response to heat) in SOM4, GO:0007568 (aging), GO:0071215 (cellular response to abscisic acid stimulus), GO:0006972 (hyperosmotic response) and GO:0010150 (leaf senescence) in SOM7 and GO:0009727 (detection of ethylene stimulus) and GO:0042742 (defense response to bacterium) in SOM8. GO:0071365 (cellular

response to auxin stimulus) was also enriched in SOM8 (Fig. 8c). SOM6 and 9 genes upregulated in *sh1-1* included photosynthesis-related terms such as GO:0009773 (photosynthetic electron transport in photosystem I) in SOM6 and GO:0015996 (chlorophyll catabolic process) in SOM9. Stress-related terms also appeared in SOM9, including

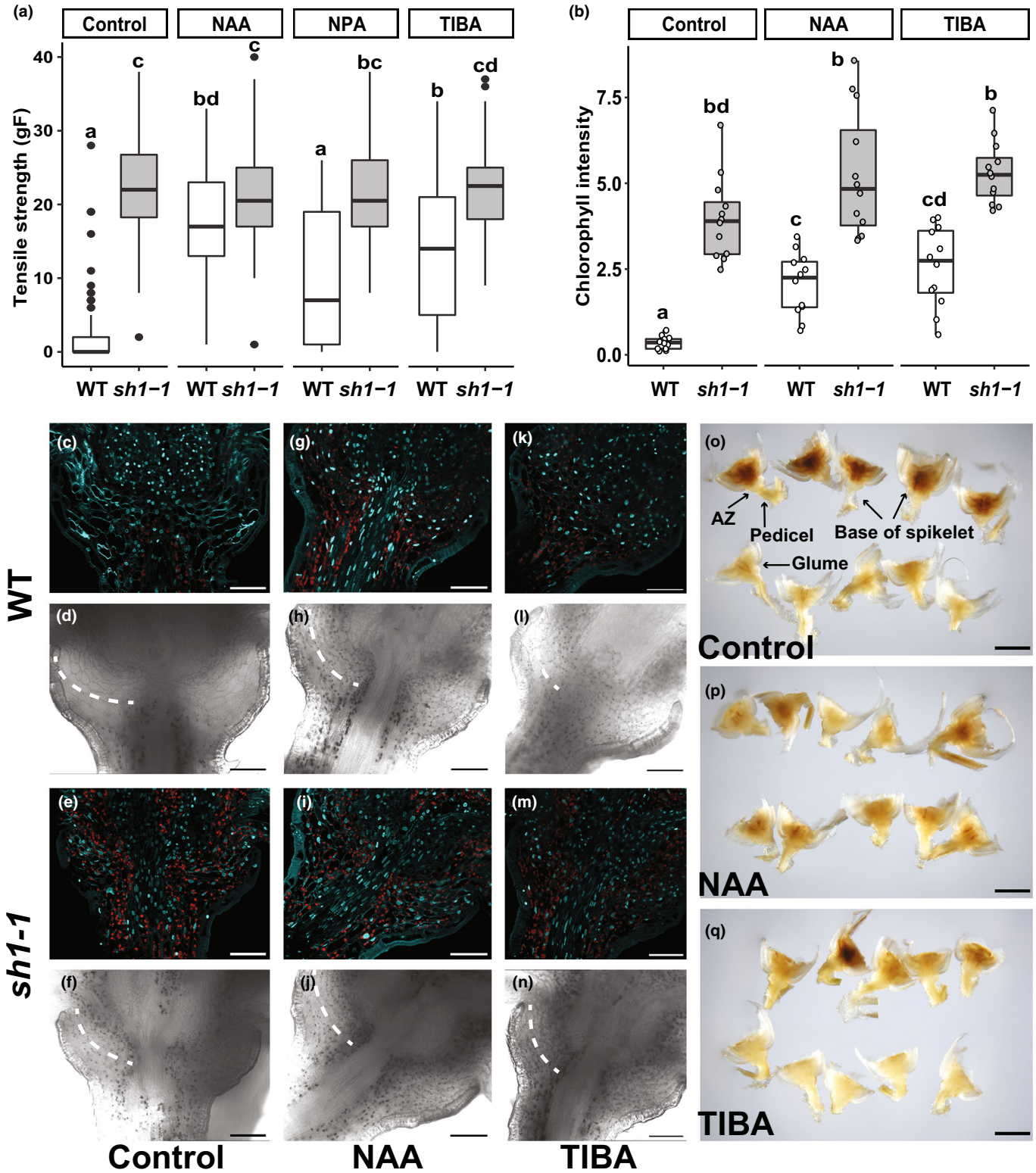

Fig. 6 Auxin signaling suppresses abscission in wild-type (WT) *Setaria viridis* via inhibiting chloroplast degradation and reactive oxygen species (ROS) accumulation. (a) Tensile strength measurements of the spikelets in WT and *shattering1-1* (*sh1-1*) mutants under various treatments. Values are 90 measurements per genotype per stage from three biological replicates in control, 1-naphthaleneacetic acid (NAA), N-1-naphthylphthalamic acid and 2,3,5-triiodobenzoic acid (TIBA) treatments. (b) Quantification of chlorophyll autofluorescence in control, NAA or TIBA treatment. Circles are individual measurements of half of the AZ. $n = 12$ from six biological abscission zone (AZ) samples per genotype per condition. Elements in the boxplot: center line, median; box limits, upper and lower quartiles; whiskers, 1.5× interquartile range; black filled circles, outliers of individual measurements. Significant differences between genotypes and conditions (Tukey's HSD test, $P < 0.01$) are indicated with different letters. (c–n) Representatives of (c, e, g, i, k, m) fluorescence and (d, f, h, j, l, n) transmitted light images of longitudinal views of AZ in (c, d, g, h, k, l) WT and (e, f, i, j, m, n) *sh1-1* under (c–f) control, (g–j) NAA and (k–n) TIBA conditions. Bars, 50 μm. Dotted white line shows approximate position of one side of the AZ. (c, e, g, i, k, m) Red color, chlorophyll autofluorescence; cyan color, DAPI and Calcofluor White signal. (o–q) 3, 3′-diaminobenzidine (DAB) staining of AZ and surrounding tissues in (o) control, (p) NAA and (q) TIBA treatments. Bars, 500 μm.

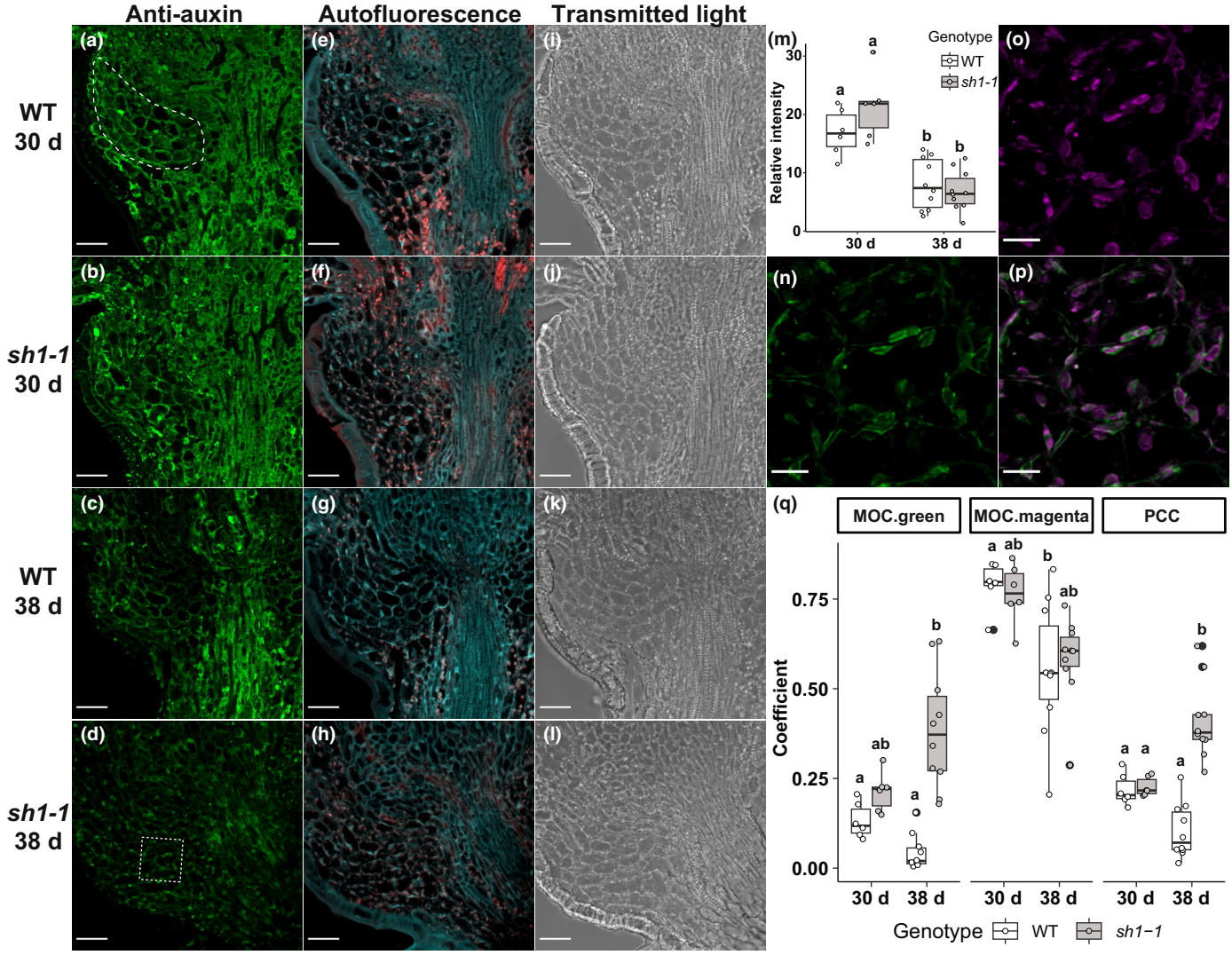

Fig. 7 Auxin is located in the chloroplast of abscission zone (AZ) in *shattering1-1* (*sh1-1*) in late development of *Setaria viridis*. (a–l) Representative immunofluorescence of (a–d) anti-auxin signal, (e–h) autofluorescence and (i–l) transmitted light images of longitudinal sections of AZ in (a, c, e, g, i, k) wild-type (WT) and (b, d, f, h, j, l) *sh1-1* at (a, b, e, f, i, j) 30 d and (c, d, g, h, k, l) 38 d. Representative measured AZ region is marked with white circle with dotted line. Bars, 25 μm. (e–h) Red color, chlorophyll autofluorescence; cyan color, cell autofluorescence. (m) Quantification of auxin signals. Circles are individual measurements of half of the AZ as shown in (a–d). Elements in the boxplot: center line, median; box limits, upper and lower quartiles; whiskers, 1.5× interquartile range. $n = 6$–10 biological samples per genotype per stage. Significant differences between genotypes and conditions (Tukey's HSD test, $P < 0.01$) are indicated with different letters. (n–p) Representative enlarged super-resolution fluorescence images of (n) auxin signal, (o) chlorophyll autofluorescence and (p) merged signal in *sh1-1* at 38 d as marked in the white box in (d). Bars, 5 μm. (q) Quantification of the overlap of green and magenta channels by Manders overlap coefficient (MOC) and Pearson's correlation coefficient (PCC). MOC.green and MOC.magenta refer to the proportion of overlapped signal to the total green and magenta signal, respectively. Circles are values calculated from individual samples. Elements in the boxplot as in (m). The same biological samples as in (m) were used for overlap quantification. Significant differences between genotypes and conditions (Tukey's HSD test, $P < 0.01$) are indicated with different letters.

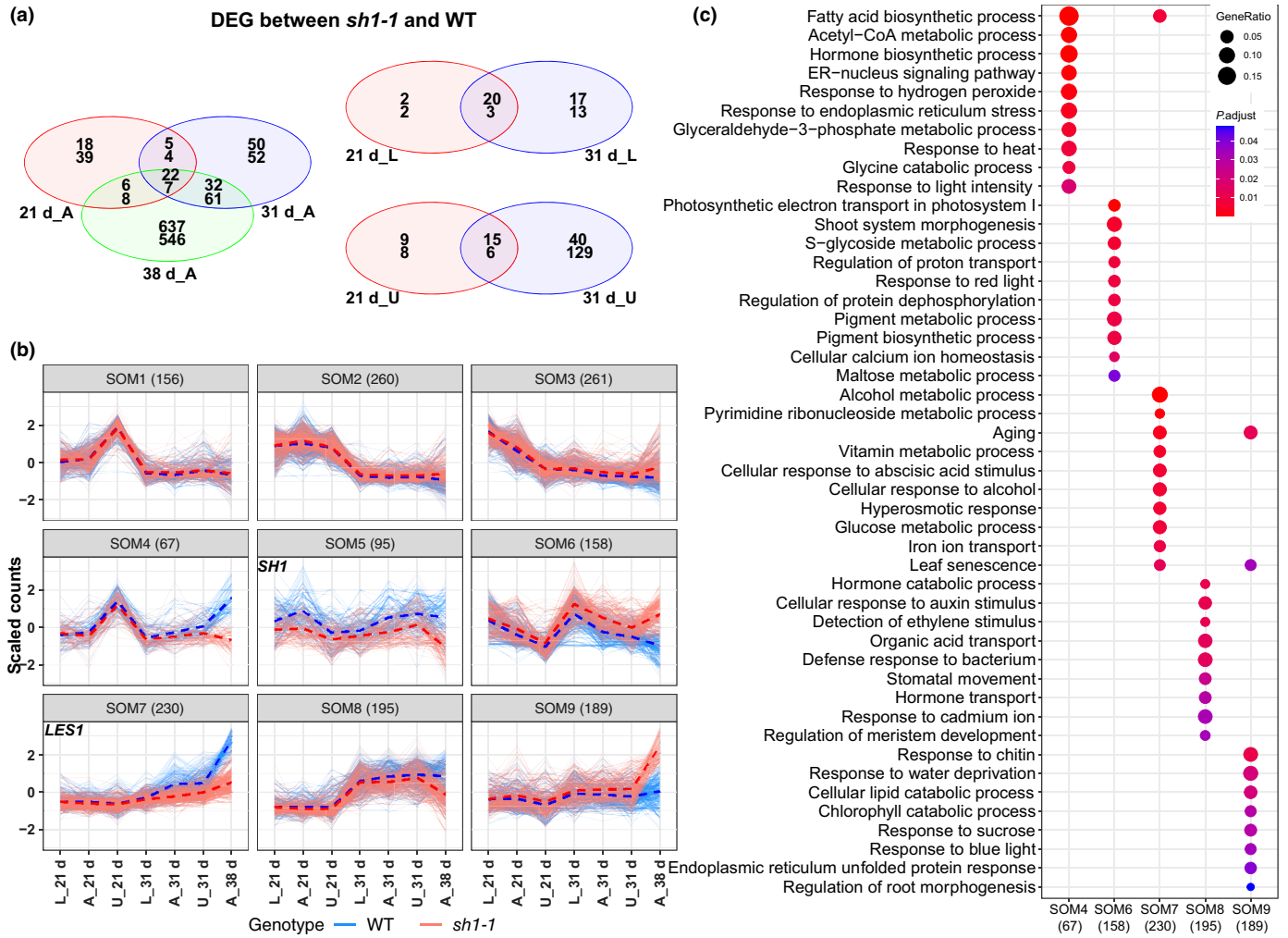

Fig. 8 Differentially expressed genes (DEGs) between wild-type (WT) *Setaria viridis* and *shattering1-1* (*sh1-1*) are more abundant in the abscission zone (AZ) in late development. (a) Venn diagrams showing up (upper numbers) and downregulated (lower numbers) genes of *sh1-1* vs WT at 21, 31 and 38 d. A, AZ; L, lower tissue of the AZ (pedicel); U, upper tissue of the AZ (base of the spikelet). (b) Self-Organizing Map (SOM) clusters of DEGs. The number of genes in each cluster is indicated in parentheses. Each cluster includes genes with similar patterns of expression, with tissues and time points arranged along the *x*-axis, expression levels on the *y*-axis. Fine solid lines, expression patterns of each gene; heavy dotted lines, average expression patterns of the genes in each cluster within the genotype. Blue, WT; red, *sh1-1*. When expression patterns in mutant and WT are similar, the red and blue lines are similar in pattern (SOM1, 2, 3), whereas if WT expression is higher, the blue lines appear above the red ones (SOM4, 5, 7, 8) and vice versa (SOM6, 9). (c) Top 10 most significant gene ontology (GO) terms enriched in each cluster. Red and blue represent smaller and larger adjusted *P*-values, respectively. The size of the dots represents the ratio of genes in each GO term over the total number of genes in the cluster.

GO:0007568 (aging), GO:0009414 (response to water deprivation), GO:0010150 (leaf senescence) and GO:0030968 (endoplasmic reticulum unfolded protein response; Fig. 8c).

Of the eight DEGs in the lignin biosynthetic pathway reported by Liu *et al.* (2022), only a NAC transcription factor (Sevir.6G085750) was differentially expressed in our dataset. This gene was downregulated in the AZ at 38 d in our samples, but was reported as upregulated by Liu *et al.* (2022). We searched for other lignin-related genes in our DEGs and identified a Caffeoyl-CoA *O*-methyltransferase (Sevir.6G204900) and a laccase (Sevir.5G388000) downregulated in the AZ of *sh1-1* at 38 and 21 d, respectively. Additionally, two pectinacetylesterases (Sevir.5G079400 and Sevir.9G336500) and one polygalacturonase (Sevir.3G165200) were downregulated, and nine glucosidase/glucanase-related genes were differentially expressed in the AZ of *sh1-1* at 38 d (Table S2).

Auxin-related genes were differentially regulated in the AZ of *sh1*

Our hormonal treatments, IAA localization and RNA-Seq analysis suggested that *SH1* may regulate shattering through auxin pathways (Figs 6, 7, 8c). We therefore specifically examined auxin-related DEGs. The term 'auxin response' was enriched in SOM8, in which genes were downregulated at 38 d in *sh1-1* (Fig. 8b,c), although other auxin-related DEGs were found in other SOMs. In total, 29 auxin-related DEGs were variously up and downregulated in the mutant, including genes involved in

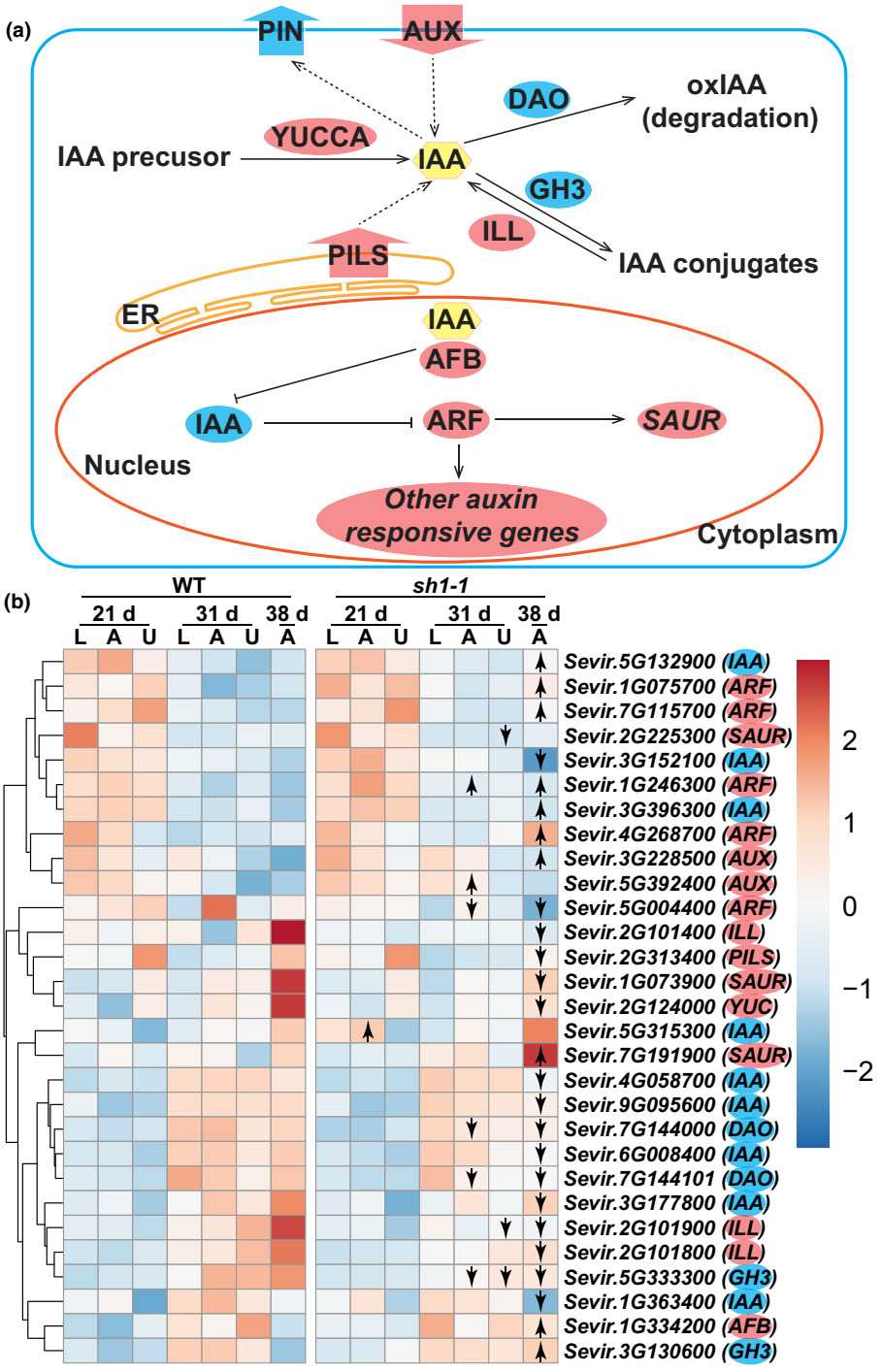

Fig. 9 Auxin-related genes are differentially expressed between wild-type (WT) and *shattering1-1* (*sh1-1*) in the abscission zone (AZ) of *Setaria viridis*. (a) A diagram illustrating differentially expressed genes between WT and *sh1-1* involved in auxin transport, homeostasis and signaling in a cell. Auxin transporters include exporters PIN localized on the plasma membrane and PIN-LIKES (PILS) localized on the endoplasmic reticulum (ER) membrane, and importer AUX. Dashed arrows indicate the direction of IAA movement. Auxin homeostasis proteins include indole-3-acetic acid (IAA) biosynthetic enzyme YUCCA, DIOXYGENASE OF AUXIN OXIDATION (DAO), auxin amide conjugate synthetase GRETCHEN HAGEN 3 (GH3) and IAA-amino hydrolase IAA-LEUCINE RESISTANT-LIKE (ILL). Auxin signaling proteins include AUXIN RESPONSE FACTORs (ARFs), AUXIN/INDOLEACETIC ACID (AUX/IAAs), SMALL AUXIN UP RNAs (SAURs) and AUXIN SIGNALING F-BOX PROTEIN (AFB). Blunt-ended arrows indicate negative regulation and headed arrows indicate positive regulation. (b) Gene expression heatmap of auxin-related genes normalized by each gene from the RNA-Seq experiment. Significant differential expression between *sh1-1* and WT (1.5-fold change; Wald test, adjusted *P*-value < 0.05) is indicated by arrows. Arrowheads up and down denote upregulation and downregulation in the mutant, respectively. Proteins leading to increased free IAA or positive regulators of auxin signaling are in red, and proteins leading to decreased free IAA or auxin response repressors are in blue. A, AZ; L, lower tissue of the AZ; U, upper tissue of the AZ.

auxin signaling, metabolism and transport that may positively or negatively impact auxin signaling (Fig. 9; Rosquete *et al.*, 2012; Zhang & Peer, 2017; Sauer & Kleine-Vehn, 2019; Yu *et al.*, 2022). Most differences were observed late in development. In mutant plants at 38 d, auxin signaling DEGs included five *AUXIN RESPONSE FACTORs* (*ARFs*; four upregulated and one downregulated), eight *AUXIN/INDOLEACETIC ACID* (*AUX/IAAs*; two upregulated and six downregulated), three *SMALL AUXIN UP RNAs* (*SAURs*; one upregulated and two downregulated) and one *AUXIN SIGNALING F-BOX PROTEIN* (*AFB*; upregulated). Among auxin metabolism genes, an auxin biosynthetic enzyme *YUCCA* (*YUC*) was downregulated; two *GRETCHEN HAGEN 3* (*GH3*) encoding auxin amide conjugate synthetases were up and downregulated; all three *IAA-LEUCINE RESISTANT-LIKE* (*ILL*) of IAA amidohydrolases and two *DIOXYGENASE OF AUXIN OXIDATION* (*DAO*) were downregulated. Among auxin transport genes, two auxin influx carriers (*AUX*) were upregulated, while one efflux carrier *PIN-LIKES* (*PILS*) was downregulated (Fig. 9). The differential expression of these genes could lead to either more or less free IAA, suggesting

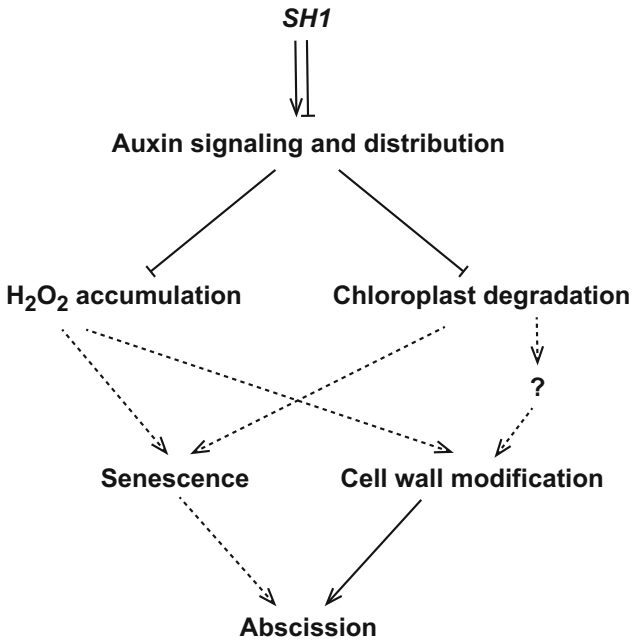

Fig. 10 Putative model of *SHATTERING1* (*SH1*) regulating the activation of abscission in *Setaria viridis*. *SH1* regulates auxin signaling and distribution, which inhibits H_2O_2 accumulation and chloroplast degradation, two indicators of organ senescence. H_2O_2 accumulation and chloroplast degradation also precede abscission. In addition, cell wall is modified during the initiation of abscission. Solid lines indicate evidence from this study; dotted lines indicate literature evidence and hypothetical connection. Headed arrows indicate positive regulation and blunt-ended arrows indicate negative regulation.

that *SH1* regulation of auxin signaling and homeostasis is complex.

Discussion

The function of *YAB2/SH1* differs between rice and *Setaria*

Grass YAB genes have different expression patterns from those of eudicot species (Bowman, 2000; Juarez *et al.*, 2004; Dai *et al.*, 2007; Tanaka *et al.*, 2012; Yu *et al.*, 2020a), and the control of shattering by *YAB2/SH1* has only been reported in grasses to date. Most known shattering genes in grasses involve early development of the AZ and control morphology and lignification patterns, which differ considerably among grass species (Li & Olsen, 2016; Yu & Kellogg, 2018; Yu *et al.*, 2020a,b). As these genes predetermine the AZ, discovery of later events that activate abscission is obscured, and therefore, little is known about the activation process in the family. In this study, we focused on *SH1*, which controls shattering in multiple grass species including ones with diverse AZ anatomy. We demonstrated that in *S. viridis*, *SvSH1* is required for activation of abscission via auxin signaling and homeostasis, ROS production and chloroplast degradation (Fig. 10), pathways that are not described for abscission in rice or any other grasses (Lv *et al.*, 2017; Li *et al.*, 2020). Although Liu *et al.* (2022) reported lignin biosynthetic genes to be regulated by SvSH1, with *CAD2* as a direct target, lignin is unlikely to be involved in abscission in *S. viridis*, in that AZs are nonlignified in WT A10 and ME034V backgrounds, the *Svsh1* mutants, and the domesticated *S. italica* (Figs 2, S5; Hodge & Kellogg, 2016; Mamidi *et al.*, 2020; Liu *et al.*, 2022). Our RNA-Seq data, which are specific to the AZ, did not find the same DEGs reported by Liu *et al.* (2022; Table S2) in their analyses of whole panicles, implying that any lignification happened in tissues other than the abscission zone. The differences between their study and ours may also reflect different sampled tissue types, genetic background, growth conditions and/or developmental stages.

YABs may function through auxin dynamics and signaling

The connection between auxin signaling and YAB function has not been reported previously in grasses. Auxin levels in the AZ did not differ between WT and *Svsh1* mutants at both 31 and 38 d, assayed by immunofluorescence (Fig. 7a–m). However, at 38 d, more of the signal was localized in the chloroplast of the mutant (Figs 7n–q, S8). The antibody used here not only has high cross-reactivity with IAA but also reacts weakly with its conjugated derivatives (Pence & Caruso, 1987; Avsian-Kretchmer *et al.*, 2002); therefore, we cannot differentiate different forms of auxin. Our RNA-Seq analysis found DEGs that may lead to increased free IAA content in *sh1-1* through transport, conjugation or oxidation pathways, such as upregulation of *AUX* and downregulation of *GH3* and *DAO*, and DEGs that may lead to reduced free IAA, such as downregulation of *PILS*, *YUC* and *ILLs*, which decrease intracellular auxin export, biosynthesis and hydrolysis of IAA conjugates to free IAA, respectively. We also found both up and downregulation of auxin signaling genes (Fig. 9). We explored potential direct targets of SH1 using public data on YABBY-binding motifs in *Arabidopsis* and soybean from -protein-binding microarray, DNA affinity purification sequencing (DAP-Seq) or Chromatin Immunoprecipitation Sequencing (ChIP-Seq; Shamimuzzaman & Vodkin, 2013; Franco-Zorrilla *et al.*, 2014; O'Malley *et al.*, 2016). Most auxin-related DEGs have at least one putative YAB-binding motif in their promoters (Table S5), but these motifs are not well conserved, so any conclusion will require experimental validation. We conclude that the *SvSH1* mutation affects auxin dynamics in the AZ, but future studies are required to elucidate the specific auxin pathways and whether the regulation is through direct targeting.

Auxin signaling inhibits chloroplast degradation in regulation of abscission in *S. viridis*

We found that auxin inhibited abscission of *S. viridis*, while GA had no effect (Figs 6a, S6), as previously reported (Weiser *et al.*, 1979; Sargent *et al.*, 1984). In our conditions, ethylene and ABA treatments suppressed normal seed development and abscission in WT, implying that normal seed maturation may be necessary to activate abscission (Fig. S6b,c). Additionally, we found that the auxin efflux inhibitor TIBA but not NPA had an effect similar to NAA (Fig. 6). TIBA, but not NPA, interferes with vesicle trafficking and actin dynamics, suggesting that TIBA and NPA compounds may inhibit different cellular activities

(Dhonukshe *et al.*, 2008; Teale & Palme, 2017). Both adding auxin (NAA) and inhibiting its efflux (TIBA) suppress abscission, pointing to auxin distribution and dynamics, rather than absolute concentration, as activating abscission.

NAA and TIBA treatments inhibited chlorophyll breakdown and ROS generation in WT, partially mimicking the phenotype of *sh1-1*, placing auxin signaling upstream of these processes (Figs 6, 10, S7). Chloroplast degradation indicates cell death and organ senescence (van Doorn & Woltering, 2004; van Doorn *et al.*, 2011), and indeed, we observed large vacuoles and empty cells in addition to chloroplast breakdown in the AZ of WT during abscission (Fig. 5i–l). Auxin inhibition of both senescence and abscission is also reported in *Arabidopsis*. AtARF1 and 2 accelerate leaf senescence and yellowing and floral organ abscission independent of ethylene (Ellis *et al.*, 2005). Ectopic expression of Trp-2-monooxygenase, which promotes auxin production, delayed floral organ shedding and sepal yellowing (Basu *et al.*, 2013). Thus, the connection between senescence and abscission may be conserved between eudicots and grasses.

sh1 mutants flower slightly later (Fig. S2a), and their glumes and AZ stay green for much longer than WT (Fig. 4), suggesting that SH1 regulates both senescence and abscission in the AZ area. Future studies are necessary to dissect whether senescence is a prerequisite for abscission or proceeds in parallel.

In addition to the connection between auxin, senescence and abscission, auxin may also regulate chloroplast function. Our immunolabeling suggested that auxin may be localized in the chloroplasts of the mutant at late developmental stages (Fig. 7d,n–q), as also reported in *Arabidopsis* and *Coffea* by immunofluorescence (Aloni *et al.*, 2003; Márquez-López *et al.*, 2018), and in *Nicotiana*, *Pinus*, sunflower and barley by gas or liquid chromatography (Sandberg *et al.*, 1982, 1990; Fregeau & Wightman, 1983). IAA precursors, such as tryptophan and indole-3-glycerol phosphate, are synthesized in the chloroplast, but final IAA production is thought to occur in the cytosol (Ljung, 2013). It is unlikely that the antibody used in this study labeled tryptophan as the reactivity is negligible (Pence & Caruso, 1987). Additionally, IAA is detected in the chloroplast in some species by gas or liquid chromatography (Fregeau & Wightman, 1983; Sandberg *et al.*, 1990). Auxin signaling also positively regulates chloroplast development, chlorophyll content and photosynthesis, although the molecular pathway remains unclear (Salazar-Iribe & De-la-Peña, 2020). Whether such regulation involves chloroplast localized auxin requires future investigation.

Auxin signaling inhibits H_2O_2 production above the AZ in *S. viridis*

In eudicots, ROS accumulate in the AZ of *Arabidopsis* and tomato flowers, and *Capsicum* leaves (Sakamoto *et al.*, 2008; Bar-Dror *et al.*, 2011; Lee *et al.*, 2018), and are necessary to upregulate proteins required for abscission such as cellulase *Cel2* in *Capsicum*, and receptor-like kinase *HAESA* and its ligand *INFLORESCENCE DEFICIENT IN ABSCISSION* (Sakamoto *et al.*, 2008; Lee *et al.*, 2022). ROS accumulation in the *Arabidopsis* floral AZ is also necessary for lignin formation, which may facilitate abscission by restricting cell wall hydrolyzing enzymes within the AZ (Lee *et al.*, 2018). These results suggest that ROS are not just stress indicators but are also signaling molecules that promote abscission. Unlike in eudicots, we did not observe H_2O_2 or superoxide accumulation in the AZ of *S. viridis* (Figs 6o–q, S7). Due to the difficulty of substrate penetration into live tissues, we fixed and cut open the AZ tissues to expose inner cell layers, so the transient superoxide may have been lost during processing. Nonetheless, we observed strong H_2O_2 signal above the AZ in WT but not *sh1-1*, and H_2O_2 production can be partially suppressed by either NAA or TIBA treatment, indicating that SH1 regulates H_2O_2 production through auxin signaling (Fig. 10).

Acknowledgements

We acknowledge imaging support from the Advanced Bioimaging Laboratory (RRID:SCR_018951) at the Donald Danforth Plant Science Center, which houses the Leica SP8-X confocal microscope acquired through an NSF Major Research Instrumentation grant (DBI-1337680) and the Thermo Fisher Scientific Talos L120C TEM acquired through generous donor support to the Center. We thank Guangyan Li and Alexandria Pete for their contribution to *sh1* phenotyping. We thank Xiang Ji, Drs Colby Starker and Eva Konecna for making the CRISPR construct and doing initial screen of the *sh1* mutants. The study was funded by NSF-IOS 1938086 and 1938093 to EAK and AND, respectively. We thank the editor and three anonymous reviewers for constructive comments on the manuscript.

Competing interests

None declared.

Author contributions

AND and EAK designed the research and secured funding. AND, EAK and YY designed the experimental approach, and YY performed the experiments. HH and YY analyzed the RNA-Seq data, and HH analyzed the YABBY-binding motif. DFV produced the Crispr-Cas9 mutants. EAK and YY drafted the manuscript, and all authors discussed the results and edited the manuscript.

ORCID

Andrew N. Doust https://orcid.org/0000-0002-2324-5495
Hao Hu https://orcid.org/0000-0003-4986-2034
Elizabeth A. Kellogg https://orcid.org/0000-0003-1671-7447
Daniel F. Voytas https://orcid.org/0000-0002-4944-1224
Yunqing Yu https://orcid.org/0000-0003-2447-6161

Data availability

The data supporting the findings of this study are available within the paper and/or its Supporting Information. RNA-seq data are

available in the Sequence Read Archive under BioProject PRJNA939260.

References

Aloni R, Schwalm K, Langhans M, Ullrich CI. 2003. Gradual shifts in sites of free-auxin production during leaf-primordium development and their role in vascular differentiation and leaf morphogenesis in *Arabidopsis*. *Planta* **216**: 841–853.

Atmodjo MA, Hao Z, Mohnen D. 2013. Evolving views of pectin biosynthesis. *Plant Biology* **64**: 747–779.

Avni R, Nave M, Barad O, Baruch K, Twardziok SO, Gundlach H, Hale I, Mascher M, Spannagl M, Wiebe K *et al.* 2017. Wild emmer genome architecture and diversity elucidate wheat evolution and domestication. *Science* **357**: 93–97.

Avsian-Kretchmer O, Cheng J-C, Chen L, Moctezuma E, Sung ZR. 2002. Indole acetic acid distribution coincides with vascular differentiation pattern during *Arabidopsis* leaf ontogeny. *Plant Physiology* **130**: 199–209.

Bailey TL, Johnson J, Grant CE, Noble WS. 2015. The MEME suite. *Nucleic Acids Research* **43**: W39–W49.

Bar-Dror T, Dermastia M, Kladnik A, Znidaric MT, Novak MP, Meir S, Burd S, Philosoph-Hadas S, Ori N, Sonego L *et al.* 2011. Programmed cell death occurs asymmetrically during abscission in tomato. *Plant Cell* **23**: 4146–4163.

Basu MM, González-Carranza ZH, Azam-Ali S, Tang S, Shahid AA, Roberts JA. 2013. The manipulation of auxin in the abscission zone cells of *Arabidopsis* flowers reveals that Indoleacetic acid signaling is a prerequisite for organ shedding. *Plant Physiology* **162**: 96–106.

Boerjan W, Ralph J, Baucher M. 2003. Lignin biosynthesis. *Plant Biology* **54**: 519–546.

Bolger AM, Lohse M, Usadel B. 2014. Trimmomatic: a flexible trimmer for Illumina sequence data. *Bioinformatics* **30**: 2114–2120.

Bowman JL. 2000. The YABBY gene family and abaxial cell fate. *Current Opinion in Plant Biology* **3**: 17–22.

Dai M, Hu Y, Zhao Y, Liu H, Zhou D-X. 2007. A WUSCHEL-LIKE HOMEOBOX gene represses a YABBY gene expression required for rice leaf development. *Plant Physiology* **144**: 380–390.

Dhonukshe P, Grigoriev I, Fischer R, Tominaga M, Robinson DG, Hašek J, Paciorek T, Petrášek J, Seifertová D, Tejos R *et al.* 2008. Auxin transport inhibitors impair vesicle motility and actin cytoskeleton dynamics in diverse eukaryotes. *Proceedings of the National Academy of Sciences, USA* **105**: 4489–4494.

Ding B, Li J, Gurung V, Lin Q, Sun X, Yuan Y. 2021. The leaf polarity factors SGS3 and YABBYs regulate style elongation through auxin signaling in *Mimulus lewisii*. *New Phytologist* **232**: 2191–2206.

Dobin A, Davis CA, Schlesinger F, Drenkow J, Zaleski C, Jha S, Batut P, Chaisson M, Gingeras TR. 2013. Star: ultrafast universal RNA-Seq aligner. *Bioinformatics* **29**: 15–21.

Dong Y, Wang Y-Z. 2015. Seed shattering: from models to crops. *Frontiers in Plant Science* **6**: 476.

van Doorn WG, Beers EP, Dangl JL, Franklin-Tong VE, Gallois P, Hara-Nishimura I, Jones AM, Kawai-Yamada M, Lam E, Mundy J *et al.* 2011. Morphological classification of plant cell deaths. *Cell Death & Differentiation* **18**: 1241–1246.

van Doorn WG, Woltering EJ. 2004. Senescence and programmed cell death: substance or semantics? *Journal of Experimental Botany* **55**: 2147–2153.

Dunn KW, Kamocka MM, McDonald JH. 2011. A practical guide to evaluating colocalization in biological microscopy. *American Journal of Physiology-Cell Physiology* **300**: C723–C742.

Ellis CM, Nagpal P, Young JC, Hagen G, Guilfoyle TJ, Reed JW. 2005. AUXIN RESPONSE FACTOR1 and AUXIN RESPONSE FACTOR2 regulate senescence and floral organ abscission in *Arabidopsis thaliana*. *Development* **132**: 4563–4574.

Ferrándiz C, Liljegren SJ, Yanofsky MF. 2000. Negative regulation of the *SHATTERPROOF* genes by FRUITFULL during *Arabidopsis* fruit development. *Science* **289**: 436–438.

Franco-Zorrilla JM, López-Vidriero I, Carrasco JL, Godoy M, Vera P, Solano R. 2014. DNA-binding specificities of plant transcription factors and their potential to define target genes. *Proceedings of the National Academy of Sciences, USA* **111**: 2367–2372.

Fregeau JA, Wightman F. 1983. Natural occurrence and biosynthesis of auxins in chloroplast and mitochondrial fractions from sunflower leaves. *Plant Science Letters* **32**: 23–34.

Gil-Humanes J, Wang Y, Liang Z, Shan Q, Ozuna CV, Sánchez-León S, Baltes NJ, Starker C, Barro F, Gao C *et al.* 2017. High-efficiency gene targeting in hexaploid wheat using DNA replicons and CRISPR/Cas9. *The Plant Journal* **89**: 1251–1262.

Hodge JG, Kellogg EA. 2016. Abscission zone development in *Setaria viridis* and its domesticated relative, *Setaria italica*. *American Journal of Botany* **103**: 998–1005.

Juarez MT, Twigg RW, Timmermans MCP. 2004. Specification of adaxial cell fate during maize leaf development. *Development* **131**: 4533–4544.

Kakei Y, Yamazaki C, Suzuki M, Nakamura A, Sato A, Ishida Y, Kikuchi R, Higashi S, Kokudo Y, Ishii T *et al.* 2015. Small-molecule auxin inhibitors that target YUCCA are powerful tools for studying auxin function. *The Plant Journal* **84**: 827–837.

Kim J. 2014. Four shades of detachment: regulation of floral organ abscission. *Plant Signaling & Behavior* **9**: e976154.

Kim J, Dotson B, Rey C, Lindsey J, Bleecker AB, Binder BM, Patterson SE. 2013. New clothes for the jasmonic acid receptor COI1: delayed abscission, meristem arrest and apical dominance. *PLoS ONE* **8**: e60505.

Knapp E, Flores R, Scheiblin D, Scheiblin D, Modla S, Czymmek K, Czymmek K, Yusibov V. 2012. A cryohistological protocol for preparation of large plant tissue sections for screening intracellular fluorescent protein expression. *BioTechniques* **52**: 31–37.

Konishi S, Izawa T, Lin SY, Ebana K, Fukuta Y, Sasaki T, Yano M. 2006. An SNP caused loss of seed shattering during rice domestication. *Science* **312**: 1392–1396.

Lee J, Chen H, Lee G, Emonet A, Kim S, Shim D, Lee Y. 2022. MSD2-mediated ROS metabolism fine-tunes the timing of floral organ abscission in *Arabidopsis*. *New Phytologist* **235**: 2466–2480.

Lee Y, Yoon TH, Lee J, Jeon SY, Lee JH, Lee MK, Chen H, Yun J, Oh SY, Wen X *et al.* 2018. A lignin molecular brace controls precision processing of cell walls critical for surface integrity in *Arabidopsis*. *Cell* **173**: 1468–1480.

Lenser T, Theißen G. 2013. Conservation of fruit dehiscence pathways between *Lepidium campestre* and *Arabidopsis thaliana* sheds light on the regulation of *INDEHISCENT*. *The Plant Journal* **76**: 545–556.

Leverone LA, Stroup TL, Caruso JL. 1991. Western blot analysis of cereal grain prolamins using an antibody to carboxyl-linked indoleacetic acid. *Plant Physiology* **96**: 1076–1078.

Li C, Zhou A, Sang T. 2006. Rice domestication by reducing shattering. *Science* **311**: 1936–1939.

Li F, Komatsu A, Ohtake M, Eun H, Shimizu A, Kato H. 2020. Direct identification of a mutation in *OsSh1* causing non-shattering in a rice (*Oryza sativa* L.) mutant cultivar using whole-genome resequencing. *Scientific Reports* **10**: 14936.

Li K, Reeve DW. 2005. Fluorescent labeling of lignin in the wood pulp fiber wall. *Journal of Wood Chemistry and Technology* **24**: 169–181.

Li L-F, Olsen KM. 2016. To have and to hold: selection for seed and fruit retention during crop domestication. *Current Topics in Developmental Biology* **119**: 63–109.

Liljegren SJ, Roeder AHK, Kempin SA, Gremski K, Østergaard L, Guimil S, Reyes DK, Yanofsky MF. 2004. Control of fruit patterning in *Arabidopsis* by INDEHISCENT. *Cell* **116**: 843–853.

Lin Z, Li X, Shannon LM, Yeh C-T, Wang ML, Bai G, Peng Z, Li J, Trick HN, Clemente TE *et al.* 2012. Parallel domestication of the *Shattering1* genes in cereals. *Nature Genetics* **44**: 720–724.

Liu H, Fang X, Zhou L, Li Y, Zhu C, Liu J, Song Y, Jian X, Xu M, Dong L *et al.* 2022. Transposon insertion drove the loss of natural seed shattering during Foxtail Millet domestication. *Molecular Biology and Evolution* **39**: msac078.

Ljung K. 2013. Auxin metabolism and homeostasis during plant development. *Development* **140**: 943–950.

Love MI, Huber W, Anders S. 2014. Moderated estimation of fold change and dispersion for RNA-seq data with DESeq2. *Genome Biology* **15**. doi: 10.1186/s13059-014-0550-8.

Lv S, Wu W, Wang M, Meyer RS, Ndjiondjop M-N, Tan L, Zhou H, Zhang J, Fu Y, Cai H *et al.* 2017. Genetic control of seed shattering during African rice domestication. *Nature Plants* **4**: 331–337.

Mamidi S, Healey A, Huang P, Grimwood J, Jenkins J, Barry K, Sreedasyam A, Shu S, Lovell JT, Feldman M *et al.* 2020. A genome resource for green millet, *Setaria viridis*, enables discovery of agronomically valuable loci. *Nature Biotechnology* **38**: 1203–1210.

Mann DGJ, LaFayette PR, Abercrombie LL, King ZR, Mazarei M, Halter MC, Poovaiah CR, Baxter H, Shen H, Dixon RA *et al.* 2012. Gateway-compatible vectors for high-throughput gene functional analysis in switchgrass (*Panicum virgatum* L.) and other monocot species. *Plant Biotechnology Journal* **10**: 226–236.

Márquez-López RE, Pérez-Hernández C, Ku-González Á, Galaz-Ávalos RM, Loyola-Vargas VM. 2018. Localization and transport of indole-3-acetic acid during somatic embryogenesis in *Coffea canephora*. *Protoplasma* **255**: 695–708.

Mohnen D. 2008. Pectin structure and biosynthesis. *Current Opinion in Plant Biology* **11**: 266–277.

Odonkor S, Choi S, Chakraborty D, Martinez-Bello L, Wang X, Bahri BA, Tenaillon MI, Panaud O, Devos KM. 2018. QTL mapping combined with comparative analyses identified candidate genes for reduced shattering in *Setaria italica*. *Frontiers in Plant Science* **9**: 918.

O'Malley RC, Huang SC, Song L, Lewsey MG, Bartlett A, Nery JR, Galli M, Gallavotti A, Ecker JR. 2016. Cistrome and epicistrome features shape the regulatory DNA landscape. *Cell* **165**: 1280–1292.

Patterson SE. 2001. Cutting loose. Abscission and dehiscence in *Arabidopsis*. *Plant Physiology* **126**: 494–500.

Patterson SE, Bleecker AB. 2004. Ethylene-dependent and -independent processes associated with floral organ abscission in *Arabidopsis*. *Plant Physiology* **134**: 194–203.

Pence VC, Caruso JL. 1987. Immunoassay methods of plant hormone analysis. In: Davies PJ, ed. *Plant hormones and their role in plant growth and development*. Dordrecht, the Netherland: Springer, 240–256.

Polko JK, Kieber JJ. 2019. The regulation of cellulose biosynthesis in plants. *Plant Cell* **31**: 282–296.

Pourkheirandish M, Hensel G, Kilian B, Senthil N, Chen G, Sameri M, Azhaguvel P, Sakuma S, Dhanagond S, Sharma R *et al.* 2015. Evolution of the grain dispersal system in barley. *Cell* **162**: 527–539.

Rosquete MR, Barbez E, Kleine-Vehn J. 2012. Cellular auxin homeostasis: gatekeeping Is housekeeping. *Molecular Plant* **5**: 772–786.

Sakamoto M, Munemura I, Tomita R, Kobayashi K. 2008. Involvement of hydrogen peroxide in leaf abscission signaling, revealed by analysis with an *in vitro* abscission system in *Capsicum* plants. *The Plant Journal* **56**: 13–27.

Salazar-Iribe A, De-la-Peña C. 2020. Auxins, the hidden player in chloroplast development. *Plant Cell Reports* **39**: 1595–1608.

Sandberg G, Gardeström P, Sitbon F, Olsson O. 1990. Presence of indole-3-acetic acid in chloroplasts of *Nicotiana tabacum* and *Pinus sylvestris*. *Planta* **180**: 562–568.

Sandberg G, Jensen E, Crozier A. 1982. Biosynthesis of indole-3-acetic acid in protoplasts, chloroplasts and a cytoplasmic fraction from barley (*Hordeum vulgare* L.). *Planta* **156**: 541–545.

Sargent JA, Osborne DJ, Dunford SM. 1984. Cell separation and its hormonal control during fruit abscission in the Gramineae. *Journal of Experimental Botany* **35**: 1663–1674.

Sarojam R, Sappl PG, Goldshmidt A, Efroni I, Floyd SK, Eshed Y, Bowman JL. 2010. Differentiating *Arabidopsis* shoots from leaves by combined YABBY activities. *Plant Cell* **22**: 2113–2130.

Sauer M, Kleine-Vehn J. 2019. PIN-FORMED and PIN-LIKES auxin transport facilitators. *Development* **146**: dev168088.

Scheller HV, Ulvskov P. 2010. Hemicelluloses. *Annual Review of Plant Biology* **61**: 263–289.

Schindelin J, Arganda-Carreras I, Frise E, Kaynig V, Longair M, Pietzsch T, Preibisch S, Rueden C, Saalfeld S, Schmid B *et al.* 2012. FIJI: an open-source platform for biological-image analysis. *Nature Methods* **9**: 676–682.

Sexton R, Roberts JA. 1982. Cell biology of abscission. *Annual Review of Plant Physiology* **33**: 133–162.

Shamimuzzaman M, Vodkin L. 2013. Genome-wide identification of binding sites for NAC and YABBY transcription factors and co-regulated genes during soybean seedling development by ChIP-Seq and RNA-Seq. *BMC Genomics* **14**: 477.

Sun M, Li H, Li Y, Xiang H, Liu Y, He Y, Qi M, Li T. 2020. Tomato YABBY2b controls plant height through regulating indole-3-acetic acid-amido synthetase (GH3.8) expression. *Plant Science* **297**: 110530.

Tanaka W, Toriba T, Ohmori Y, Yoshida A, Kawai A, Mayama-Tsuchida T, Ichikawa H, Mitsuda N, Ohme-Takagi M, Hirano H-Y. 2012. The *YABBY* Gene *TONGARI-BOUSHI1* is involved in lateral organ development and maintenance of meristem organization in the rice spikelet. *Plant Cell* **24**: 80–95.

Teale W, Palme K. 2017. Naphthylphthalamic acid and the mechanism of polar auxin transport. *Journal of Experimental Botany* **69**: 303–312.

Van Eck J, Swartwood K, Pidgeon K, Maxson-Stein K. 2017. *Agrobacterium tumefaciens*-mediated transformation of *Setaria viridis*. In: Doust AD, Diao X, eds. *Genetics and genomics of Setaria*. Cham, Switzerland: Springer, 343–356.

Vanholme R, Meester BD, Ralph J, Boerjan W. 2019. Lignin biosynthesis and its integration into metabolism. *Current Opinion in Biotechnology* **56**: 230–239.

Wehrens R, Buydens LMC. 2007. Self- and super-organizing maps in R: the KOHONEN package. *Journal of Statistical Software* **21**: 1–19.

Weiser GC, Smith RL, Varnell RJ. 1979. Spikelet abscission in guineagrass as influenced by auxin and gibberellin 1. *Crop Science* **19**: 231–235.

Weng J, Chapple C. 2010. The origin and evolution of lignin biosynthesis. *New Phytologist* **187**: 273–285.

Woodson JD. 2022. Control of chloroplast degradation and cell death in response to stress. *Trends in Biochemical Sciences* **47**: 851–864.

Wu T, Hu E, Xu S, Chen M, Guo P, Dai Z, Feng T, Zhou L, Tang W, Zhan L *et al.* 2021. CLUSTERPROFILER 4.0: a universal enrichment tool for interpreting omics data. *The Innovations* **2**: 100141.

Yoon J, Cho L, Kim SL, Choi H, Koh H, An G. 2014. The BEL1-type homeobox gene *SH5* induces seed shattering by enhancing abscission-zone development and inhibiting lignin biosynthesis. *The Plant Journal* **79**: 717–728.

Yu Y, Beyene G, Villmer J, Duncan KE, Hu H, Johnson T, Doust AN, Taylor NJ, Kellogg EA. 2023. Grain shattering by cell death and fracture in *Eragrostis tef*. *Plant Physiology* **192**: 222–239.

Yu Y, Hu H, Doust AN, Kellogg EA. 2020a. Divergent gene expression networks underlie morphological diversity of abscission zones in grasses. *New Phytologist* **225**: 1799–1815.

Yu Y, Kellogg EA. 2018. Inflorescence abscission zones in grasses: diversity and genetic regulation. *Annual Plant Reviews* **1**: 497–532.

Yu Y, Leyva P, Tavares RL, Kellogg EA. 2020b. The anatomy of abscission zones is diverse among grass species. *American Journal of Botany* **107**: 549–561.

Yu Z, Zhang F, Friml J, Ding Z. 2022. Auxin signaling: research advances over the past 30 years. *Journal of Integrative Plant Biology* **64**: 371–392.

Zhang J, Peer WA. 2017. Auxin homeostasis: the DAO of catabolism. *Journal of Experimental Botany* **68**: 3145–3154.

Zhong R, Ye Z-H. 2015. Secondary cell walls: biosynthesis, patterned deposition and transcriptional regulation. *Plant and Cell Physiology* **56**: 195–214.

Zhou Y, Lu D, Li C, Luo J, Zhu B-F, Zhu J, Shangguan Y, Wang Z, Sang T, Zhou B *et al.* 2012. Genetic control of seed shattering in rice by the *APETALA2* transcription factor *SHATTERING ABORTION1*. *Plant Cell* **24**: 1034–1048.

Supporting Information

Additional Supporting Information may be found online in the Supporting Information section at the end of the article.

Fig. S1 Expression of *Setaria viridis SHATTERING1* (*SvSH1*) in the abscission zone of *sh1-1*.

Fig. S2 Heading date, anthesis date, inflorescence traits and plant height in the *Setaria viridis shattering1* (*Svsh1*) mutant.

Fig. S3 Allelism test in progeny of *Setaria viridis shattering1* (*Svsh1*) mutants crossed with wild-type.

Fig. S4 Spikelet histology of *Setaria viridis* genotypes.

Fig. S5 Lignification in the abscission zone of the two *Setaria viridis* genotypes.

Fig. S6 Spikelet tensile strength after hormone treatments in *shattering1-1* (*sh1-1*).

Fig. S7 H_2O_2 accumulation after auxin treatment in the two *Setaria viridis* genotypes.

Fig. S8 Antiauxin signal in *shattering1-1* (*sh1-1*) and wild-type at 38 d.

Fig. S9 Principal component analysis plot of the RNA-Seq samples.

Table S1 Statistical results from ANOVA followed by Tukey's HSD (honestly significant difference) tests.

Table S2 Results of differential gene expression analysis by DESeq2.

Table S3 Gene list of Self-Organizing Map clustering using 1611 differentially expressed genes as input.

Table S4 Gene ontology enrichment analysis of the Self-Organizing Map clusters using clusterProfiler.

Table S5 Differentially expressed genes with putative YABBY-binding motifs in their promoter.

Please note: Wiley is not responsible for the content or functionality of any Supporting Information supplied by the authors. Any queries (other than missing material) should be directed to the *New Phytologist* Central Office.